

Syracuse University

**SURFACE**

---

Theses - ALL

---

12-2013

## Raman spectroscopic investigation of chondroitinase ABC treatment after spinal cord injury in an organotypic model

Shane Ruberto

Follow this and additional works at: <https://surface.syr.edu/thesis>



Part of the [Biochemistry, Biophysics, and Structural Biology Commons](#), and the [Biomedical Engineering and Bioengineering Commons](#)

---

### Recommended Citation

Ruberto, Shane, "Raman spectroscopic investigation of chondroitinase ABC treatment after spinal cord injury in an organotypic model" (2013). *Theses - ALL*. 10.  
<https://surface.syr.edu/thesis/10>

This Thesis is brought to you for free and open access by SURFACE. It has been accepted for inclusion in Theses - ALL by an authorized administrator of SURFACE. For more information, please contact [surface@syr.edu](mailto:surface@syr.edu).

## ABSTRACT

This study investigated (1) the ability of an organotypic model of spinal cord injury (SCI) to recapitulate significant pathobiological events of *in vivo* SCI from a Raman spectroscopic perspective, and (2) the Raman spectroscopic effects of chondroitinase ABC (cABC) treatment on said model of SCI. Tissue from mouse spinal cords was excised, sectioned, and placed into culture, before being systematically injured to induce trauma. Cultures with and without cABC treatment were assessed using Raman spectroscopy at varying times post-injury. We demonstrate that Raman spectral phenomena characteristic of SCI can be observed using an organotypic model. By comparing these phenomena with well-known cellular mechanisms of SCI, we hypothesize their correlation with apoptosis, demyelination, and upregulation of endogenous biochemicals, such as chondroitin sulfate proteoglycans (CSPGs), among others. Furthermore, we demonstrate for the first time that Raman spectral phenomena are discernable during cABC treatment of SCI. Observed spectral variations correlate to the enzymatic degradation of CSPGs, protein compositional changes, and remyelination. Multivariate regression modeling confirms changes in lipid and chondroitin sulfate concentration during SCI and its cABC treatment, and provides a semi-quantitative measure of these changes. Overall, these data establish Raman spectroscopy as a viable resource for monitoring cABC treatment of SCI.

RAMAN SPECTROSCOPIC INVESTIGATION OF CHONDROITINASE ABC  
TREATMENT AFTER SPINAL CORD INJURY IN AN ORGANOTYPIC MODEL

by

Shane M. Ruberto

B.S. Bioengineering, Syracuse University, 2011

Thesis

Submitted in partial fulfillment of the requirements for the degree of  
Master of Science in *Bioengineering*.

Syracuse University  
December 2013

Copyright © Shane Ruberto 2013  
All Rights Reserved

## **ACKNOWLEDGMENTS**

First and foremost, I would like to thank my advisor, Dr. Julie Hasenwinkel, for her guidance and counseling over the course of this work. Without her insight, this project would not have been possible. I would like to thank Dr. Joseph Chaiken, who generously offered use of his Raman spectrometer, and Dr. Sandra Hewett, who generously donated the animals used in this study. Both of who welcomed me in their laboratories and were more than accommodating, and I am incredibly grateful for it. In addition, I would like to thank Dr. Bin Deng, Dr. James Hewett, and Dr. Yan He for their guidance and assistance with developing the methodologies used in this study. Finally, I would like to thank my mother, Tracy, for unwavering love and support. Her persistence in keeping me motivated and willingness to deal with my occasionally less than cheerful moods is truly a testament of her love.

## TABLE OF CONTENTS

Acknowledgements .....	iv
Table of Contents .....	v
List of Figures and Tables .....	vi
1. Specific Aims .....	1
2. Introduction .....	2
3. Materials and Methods .....	5
3.1 Preparation of organotypic spinal cord slice cultures .....	5
3.2 In vitro SCI .....	7
3.3 Measurement of cell death .....	7
3.4 Chondroitinase ABC treatment .....	9
3.5 Raman spectroscopy of slice cultures .....	10
3.6 Raman spectroscopy of biochemical constituents .....	11
3.7 Spectroscopic data analysis .....	13
3.8 Modeling of spectroscopic data .....	13
3.9 Statistical analysis .....	16
4. Results .....	16
4.1 Viability of organotypic cultures .....	16
4.2 Cell death in response to SCI .....	17
4.3 Raman assignments .....	18
4.4 Culturing has a negligible effect on the Raman spectra of organotypic spinal tissue .....	19
4.5 Effect of SCI on the Raman spectra of organotypic spinal tissue .....	21

4.6	Effect of cABC treatment on the Raman spectra of injured organotypic spinal tissue .....	23
4.7	Success of PLS regression model.....	25
4.8	Biochemical variations in response to SCI and cABC treatment.....	25
5.	Discussion .....	29
6.	Conclusion .....	39
7.	Future Work .....	40
	References.....	43
	Vita .....	48

## LIST OF FIGURES AND TABLES

Figure 1.	Overview of organotypic culture preparation and injury .....	8
Figure 2.	Schematic of the custom-built Raman spectroscope .....	12
Figure 3.	Bar charts and micrographs of cell death .....	16
Figure 4.	Spectra of uncultured versus cultured spinal cord tissue .....	20
Figure 5.	Spectra of injured spinal tissue cultures .....	22
Figure 6.	Spectra of cABC-treated and sham-treated spinal tissue cultures .....	24
Figure 7.	Spectra of biochemical constituents .....	26
Figure 8.	Measured spectra versus fitted regression equations .....	27
Figure 9.	Bar chart of relative contributions of biochemical species to injured tissue ..	28
Figure 10.	Bar chart of relative contributions of biochemical species to cABC-treated tissue .....	29
Table 1.	Band assignments for spinal tissue spectra .....	19
Table 2.	Statistical comparison between spectra of uncultured and cultured tissue ..	20
Table 3.	Statistical comparison between spectra of SCI and control groups .....	22
Table 4.	Statistical comparison between cABC-treated and sham-treated groups ....	24
Table 5.	Percent variance explained PLS regression .....	26



## 1 SPECIFIC AIMS

1. *Using Raman spectroscopy, assess the ability of an organotypic model of spinal cord injury (SCI) to recapitulate significant pathobiological events of in vivo SCI*
2. *Using Raman spectroscopy, assess the effects of chondroitinase ABC (cABC) treatment on organotypic SCI, and whether those effects, if any, correlate to the reported enzymatic action of cABC on spinal tissue*
3. *Construct a multivariate regression model of organotypic SCI and its treatment with cABC, using the acquired Raman spectra, to quantify changes in biochemical composition*

## 2 INTRODUCTION

When the spinal cord is injured, it responds by producing an axonal inhibitory matrix referred to as the glial scar.<sup>1-3</sup> This response prevents severed axons from forming new connections across the injury site, an event that, if done incorrectly, could be devastating to functionality in the central nervous system (CNS).<sup>1-3</sup> Rather than risk a potentially detrimental reconnection, the injured spinal cord uses the scar to impede axonal regrowth and preserve its residual physical and chemical integrity. However, this preventative measure comes at a price, as many victims of spinal cord injury (SCI) consequently suffer partial or complete paralysis from failed axonal regeneration. SCI victims in the United States alone number approximately 270,000, and of those more than 99% are paralytic.<sup>4</sup> To combat SCI and its debilitating effects, numerous efforts have been made to understand the underlying mechanisms of the glial scar.<sup>5-8</sup> It is, at least in part, a function of two key events. First, axons extending into the site of injury

are demyelinated by the apoptosis of oligodendrocytes, the myelinating cells of the CNS. The apoptotic fragmentation of the oligodendrocyte membrane releases myelin-associated growth inhibitors, which, when bound to complementary receptors, prohibit axonal growth. Additionally, demyelination prevents the proper electrical conductivity necessary for neurons to signal, making communication across the injury site highly improbable.<sup>8,9</sup> Second, reactive glial cells concurrently, and vigorously, upregulate chondroitin sulfate proteoglycans (CSPGs), which are secreted to produce a CSPG-rich extracellular matrix. The chondroitin sulfate glycosaminoglycan (CS-GAG) side-chains of CSPGs then bind to complementary receptors on axons, triggering a signaling pathway to further prohibit axonal growth.<sup>9,10</sup> Thus, CSPGs act as a physical barrier, by means of sheer concentration, and chemical barrier to axon regeneration.

It is reported that CSPGs are among the most proactive of axonal inhibitory molecules.<sup>10</sup> For this reason, numerous studies have focused on anti-CSPG SCI therapies using the bacterial enzyme chondroitinase ABC (cABC).<sup>1, 11-14</sup> This enzyme catalyzes the removal of CS-GAG chains from CSPG, which in turn attenuates CSPG's inhibitory action, both as a physical and chemical barrier. However, despite the success of anti-CSPG therapies, assessment thus far has relied on immunohistochemical techniques, which require preparation of tissue and further, possibly unwanted, alteration of the tissue's chemical state (e.g. fixation and staining). In recent years, Raman spectroscopy (RS) has emerged as an effective alternative in examining tissue chemistry, one that is operable in living tissue without any necessary chemical treatments.<sup>15</sup> Without the requirement of tissue preparation, RS has appreciable potential as a clinical tool for real-time assessment of SCI treatment. Ideally, the

spectroscopic technique would be used to non-invasively monitor the chemistry of treated SCI, facilitating necessary tailoring of the treatment. This study serves as a preliminary, *in vitro* exploratory effort to the aforementioned clinical therapy. The effectiveness of RS has already been demonstrated in the assessment of SCI.<sup>16,17</sup> However, no reports to date have used RS to examine the effects of anti-CSPG treatments. To that end, we present a novel Raman spectroscopic investigation, in qualitative and semi-quantitative nature, of SCI and its treatment with chondroitinase ABC in an organotypic model.

Firstly, we demonstrate a functional model of SCI - on which our spectroscopic investigation was based - using an organotypic culture platform. The animal chosen for this model was the mouse. Organotypic cultures are tissue explants, typically in the form of thin slices, which have been placed directly into culture without modification. This style of preparation preserves the original histological and morphological structures of the tissue, allowing regional specific observations. Once in culture, organotypic slices largely maintain the ability to recapitulate *in vivo* pathobiology, despite lacking extrinsic inputs.<sup>18</sup> This has been extensively demonstrated for tissue of the CNS.<sup>19-22</sup> The organotypic culture platform was chosen, foremost, because it allows SCI to be performed entirely *in vitro*, facilitating a repeatability of injury that is amply more difficult to achieve *in vivo*.<sup>18</sup> In this study, tissue was excised from the spinal cords of mice, sectioned into uniform slices, placed into culture, and systematically injured using a weight-drop device. In this way, the mechanics of injury were precisely controlled so that the injury mode and injury severity remained uniform between groups of tissue. Whereas the mechanics of *in vivo* injury can be controlled, it can only be done so

externally, meaning internal tissue injury cannot be regulated with the same degree of precision as *in vitro* injury.<sup>18</sup> For our purposes uniformity of injury was necessary, as our assessment did not pertain to the level of injury severity. Moreover, *in vitro* injury is ethically advantageous to *in vivo* injury, as it does not necessitate post-surgical animal care. As an additional motive, organotypic cultures offer precise control over the environmental conditions of excised tissue, which allows highly repeatable treatment. Direct administration of cABC into the culture medium lessened the possibility of a non-uniform drug distribution, to which a vascularized *in vivo* environment might be conducive, thus further removing variation between groups. Secondary motives include the cost effectiveness of the platform, since there is no post-surgical care, and ease-of-use, since surgery was not required immediately prior to analysis, as is necessary in *in vivo* studies to prevent tissue decay.<sup>16</sup>

With the SCI model in place, cultures with and without cABC treatment were assessed using Raman spectroscopy at varying times post-injury. We investigated (1) the ability of an organotypic model of SCI to recapitulate significant pathobiological events of *in vivo* SCI from a spectroscopic perspective and (2) the Raman spectroscopic effects of cABC on our model of SCI, and whether those effects correlated to the reported enzymatic action of cABC on spinal tissue. These characterizations are qualitative in nature. To quantitatively supplement our spectroscopic findings, partial least squares (PLS) regression was employed to construct a multivariate model of tissue composition during SCI and its treatment. The goal of the PLS regression was to ascertain the relative contribution of predetermined reference biochemicals, intrinsic to spinal tissue, to the chemical compositional profile of

organotypic spinal tissue cultures. This was executed by finding the commonality between the spectra of the reference biochemicals and the spectra of the tissue.

### **3 MATERIALS AND METHODS**

#### *3.1 Preparation of organotypic spinal cord slice cultures*

The animal protocol was approved by the Institutional Animal Care and Use Committee (IACUC) at Syracuse University and was in compliance with the National Institutes of Health (NIH) guidelines. All following procedures were performed in a sterile laminar flow cabinet. Adult female mice (*Mus musculus*) were anesthetized with isoflurane and decapitated using a rodent and small animal guillotine. The animal was positioned ventral side up and pinned into place on an ice-cold dissection board. The skin and musculature were removed from the ventral side along the midline. The ventral half of the ribcage was removed, and all organs were cleared from the thoracic cavity to expose the vertebral column. Once exposed, the vertebral column was constantly superfused with sterile, ice-cold artificial cerebral spinal fluid (ACSF) [124 mM NaCl, 3 mM KCl, 1.25 mM KH<sub>2</sub>PO<sub>4</sub>, 4 mM MgSO<sub>4</sub>, 2 mM CaCl<sub>2</sub>, 26 mM NaHCO<sub>3</sub>, 10 mM D-glucose, 2 mM ascorbic acid, and 75 μM adenosine (Sigma, St. Louis, MO); pH 7.2] to slow the inflammatory response. To access the spinal cord, an incision was made through the pedicle on either side of the first thoracic vertebra (T1) and extended down the length of the thoracic spine, separating the vertebral bodies from the lamina. The vertebral bodies were then lifted from the cord. Using microscopic assistance, the dorsal and ventral roots were transected.

Next, the thoracic region of cord (T1-T13) was excised and placed into a petri dish containing sterile, ice-cold ACSF. The thoracic region was chosen for its uniform

cross-sectional area. The time between decapitation and submersion of the spinal cord in ACSF was minimized to within 10 minutes to ensure minimal inflammation. The cord was transferred to a separate petri dish containing 30°C low gelling temperature agarose (4% w/v in ASCF), which was immediately placed on ice to induce gelation. Once gelled, an agarose block containing the cord was cut from the bulk using a scalpel and fixed onto a metal disk with cyanoacrylate. The embedded cord was cut into 400- $\mu$ m-thick transverse slices [Fig. 1(a)] using a tissue chopper (McIlwain, ON, Canada) equipped with a Feather double-edge carbon steel blade (Ted Pella, Redding, CA). The slices were immediately transferred into sterile, ice-cold ACSF, where they were gently stripped of meninges and checked for structural quality. Any incomplete or damaged slices were discarded.

Finally, slices were transferred onto Millicell culture plate inserts (PTFE membrane, 0.4  $\mu$ m pore size; EMD Millipore, Billerica, MA) using a sterile wide-end pipette. The slices were plated three per insert, and arranged without contact between one another. The culture inserts were placed into a 6-well plate, with each well containing 1.0 mL of culture medium. Culture medium consisted of 50% minimum essential medium (MEM) with L-glutamine (Invitrogen, Carlsbad, CA), 25% normal horse serum (Invitrogen), 25% Hank's balanced salt solution (HBSS) (Invitrogen), 20 mM HEPES (Invitrogen), 6.5 g/L D-glucose (Sigma), 50  $\mu$ g/mL penicillin (Invitrogen), 50 U/ml streptomycin (Invitrogen) and was adjusted to a pH of 7.3. In this method of culturing, adapted from Stoppini et al<sup>23</sup>, tissue slices have two distinct interfaces from which they receive necessary resources, an air-to-tissue interface and a medium-to-tissue interface. Slices were allowed to passively warm to room temperature before

being placed in incubation at 37°C and 5% CO<sub>2</sub>. The cultures were incubated for a maximum of 14 days *in vitro* (DIV), and the medium was changed every 3 days.

### *3.2 In vitro SCI*

Slices were cultured for 6 DIV before inducing SCI to allow acclimation to the culture conditions. SCI was induced using a weight drop apparatus housed in a sterile laminar flow cabinet. This technique was adapted from Krassioukov et al.<sup>24</sup> A headed stainless steel pin with a 2.0 mm diameter head and 0.5 g total weight was dropped from a height of 5.0 mm onto the center of the slice [Fig. 1(a)]. The cross-sectional area of the head was sufficient to cover the entire slice surface. Immediately following injury, slices were placed back into incubation at 37°C and 5% CO<sub>2</sub>. Control slices were removed from incubation for an equivalent time period and placed back into incubation without injury. Injured (SCI) groups and uninjured control (CTL) groups were analyzed at 1, 4, and 8 day(s) post-injury (DPI) [Fig. 1(b)].

### *3.3 Measurement of cell death*

Cell death was assessed using the nucleic acid stain, propidium iodide (PI) (Invitrogen, Carlsbad, CA). PI is only permeable through the damaged membranes of non-viable cells. Upon cellular entry, PI binds to nucleic acids, causing a significant increase in its fluorescence emission maximum and a forward shift in its excitation and emission peaks. PI was dissolved in serum free medium [75% MEM with L-glutamine (Invitrogen), 25% HBSS (Invitrogen), 20 mM HEPES (Invitrogen), 6.5 g/L D-glucose (Sigma, St. Louis, MO), 50 µg/mL penicillin (Invitrogen), 50 U/ml streptomycin (Invitrogen); pH 7.3] at 5 µg/ml. Serum free medium was used to reduce the fluorescence noise generated by

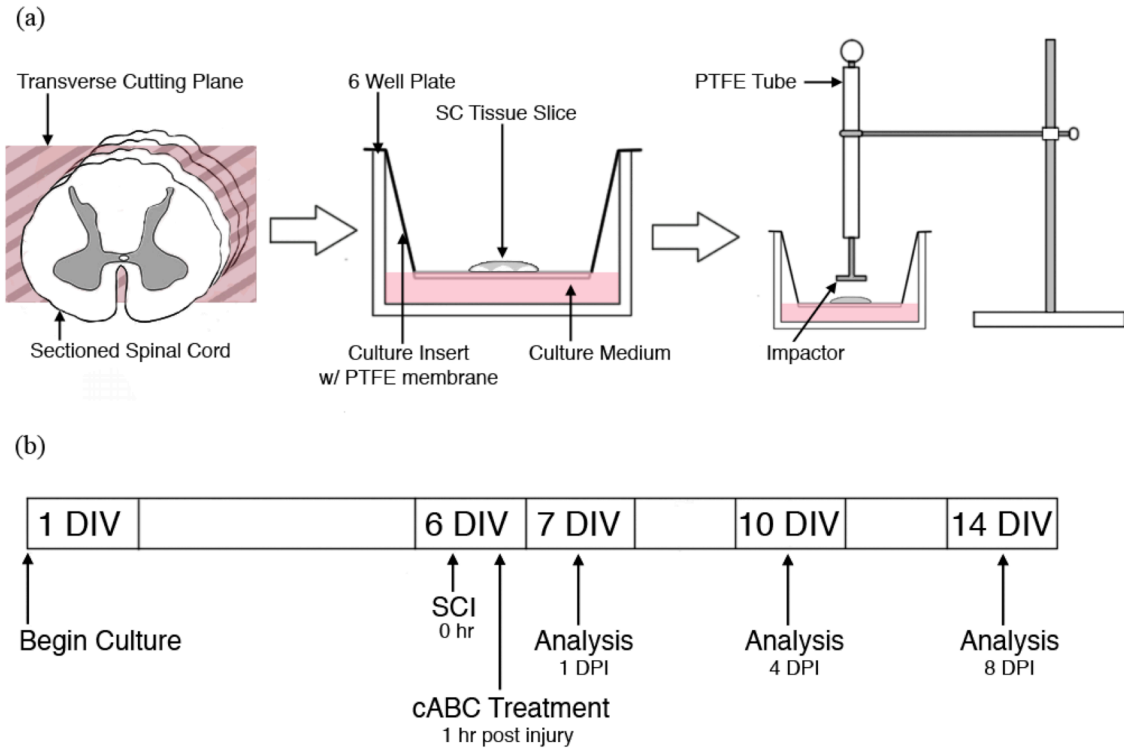


**Fig. 1** (a) Overview of organotypic culture preparation and injury. Left image shows the transverse cutting plane used to section the spinal cord; middle, the slice-interface culture method adopted from Stoppini et al.; right, the weight-drop apparatus used for injury. (b) Timeframe of experimental procedure. Cultures were allowed a period of 6 DIV before injury to ensure healing from the harvesting procedure, with injury occurring on the 6<sup>th</sup> day. One hour post-injury, cultures were treated, or not, with cABC. Spectroscopic and histological analysis was performed at 7, 10, and 14 DIV, which correspond to 1, 4, and 8 DPI.

esterase activity found in normal horse serum. Slices were removed from their current medium, gently rinsed in 1X phosphate buffered saline (PBS) to remove residual serum, and introduced to 1.0 mL PI solution.

Slices were then placed back into incubation at 37°C and 5% CO<sub>2</sub> for 1 hour to allow for permeation of PI. Fluorescence intensity was measured using a LSM 710 Confocal Microscope (Zeiss, Germany) controlled by ZEN 2010 B SPI1 software (Zeiss). PI was excited with a 543 nm Helium-Neon laser, and emissions were collected with a 605–670 nm band pass filter. A z-stack of 5 images separated by 10 μm intervals was collected in 3 non-overlapping locations for each slice using a 10X objective. The field of view,



gain, and pinhole size were standardized for all images. The mean emission intensity, a built-in function of the ZEN software, was collected for each image. Slices were then killed by submersion in 4°C PI (0.5 mg/ml solution in 1X PBS) for 72 hours. Using an identical procedure, dead slices were re-imaged to obtain a mean emission intensity that represented 100% cell death. The percent cell death for each slice was expressed as its 'alive' mean emission intensity normalized by its 'dead' mean emission intensity. To assess cell death over the duration of the culture period, groups of cultured slices (n=3) were analyzed at 1, 3, 7, 10, and 14 DIV. To assess cell death in response to SCI, SCI groups (n=3) and CTL groups (n=3) were analyzed at 1, 4, and 8 DPI. The variable 'n' refers to the number of slices.

#### *3.4 Chondroitinase ABC treatment*

Lyophilized chondroitinase ABC (cABC) (Seikagaku Corporation, Tokyo, Japan) was reconstituted in a 0.01% aqueous bovine serum albumin solution (Invitrogen, Carlsbad, CA). A buffer solution consisting of 10 U/ml reconstituted cABC, 50 mM Tris (Invitrogen), 60 mM sodium acetate (Sigma, St. Louis, MO), and 0.02% bovine serum albumin was added to culture medium for a final cABC concentration of 0.2 U/ml. This solution is referred to as cABC medium. Injured slices were cleared of culture medium and administered 1.0 ml of cABC medium 1-hour post-SCI. The cABC medium was refreshed every three days following initial treatment. Note that the *in vitro* half-life of cABC is approximately 8 days.<sup>12</sup> As a sham-control, separate groups of injured slices were administered culture medium supplemented with 2.0% 1X PBS. Groups treated with cABC (SCI +cABC) and sham-control groups treated with PBS (SCI +Sham) were analyzed at 4 and 8 DPI.

### *3.5 Raman spectroscopy of organotypic cultures*

Raman spectroscopy was performed using a custom built Raman spectroscope (Fig. 2).<sup>25</sup> For all procedures, an external cavity 785 nm laser diode (Process Instruments, Salt Lake City, Utah), adjusted to a measured power of 500 mW and spot size of 300  $\mu\text{m}$ , was used as an excitation source. Excitation light was redirected 90° from the horizontal by a periscope and passed through a pinhole located in the center of a downward facing plane mirror. Excitation light then contacted the transverse plane of the tissue slice at normal incidence, and backscatter emissions were redirected back to the horizontal direction by the plane mirror. Emissions were passed through a pair of convex lenses and into a SuperNotch laser line rejection filter (Kaiser Optical Systems, Ann Arbor, MI) before entering a HoloSpec f/1.4 spectrograph (Kaiser) equipped with a 100  $\mu\text{m}$  entrance slit. The spectrograph had a low-frequency stokes grating that operated over the spectral range -34 to 1894  $\text{cm}^{-1}$  and was coupled with a nitrogen-cooled iDus 420 series CCD Detector (Andor, Belfast, UK) to produce a spectral resolution of 2.0  $\text{cm}^{-1}$ .

Slices were cleared of culture medium and washed gently with PBS prior to imaging. Culture plate inserts containing the slices were removed from their 6-well plates and placed on an adjustable stage. Slices were positioned over an optical trap to reduce unwanted emissions. The laser focal spot was then positioned within the white matter of the spinal cord. Each spectrum was collected as 300 accumulations of 1.0-second integrations (total time of 5 minutes), and a minimum of 3 spectra was collected per slice, with each spectrum taken from a unique location within the white matter. Between acquisitions, slices were superfused with room temperature PBS to maintain

hydration. Spectra of the PTFE membrane underlying the slices were collected under identical parameters. During spectroscopic analysis, PTFE spectra were subtracted from tissue spectra to remove the Raman spectral features contributed by the PTFE membrane (See Section 3.7). All experiments were done at room temperature. Slices were discarded following analysis. To assess how the culturing of spinal cord tissue affects its Raman spectral features, a group of uncultured slices (n=3) was analyzed immediately following slicing, and groups of cultured slices (n=3) were analyzed at 6, 10, and 14 DIV. Uncultured slices underwent an identical preparation procedure to cultured slices, but were not placed in incubation and instead analyzed immediately following slicing. To assess the progression of SCI and its treatment with cABC, SCI groups (n=6) and CTL groups (n=3) were analyzed at 1, 4, and 8 DPI; and SCI +cABC groups (n=6) and SCI +Sham groups (n=3) were analyzed at 4 and 8 DPI. The variable 'n' refers to the number of slices.

### *3.6 Raman spectroscopy of biochemical constituents*

See Section 3.5 for a description of the Raman spectroscope used to perform the following experiments. Triolein ( $\geq 99\%$ ), actin (from bovine muscle), cholesterol ( $\geq 99\%$ ), collagen type IV (from calf skin), collagen type I (from calf skin), chondroitin-6-sulfate (CS-C), chondroitin-4,6-sulfate (CS-E), glial fibrillary acidic protein (GFAP), myelin basic protein ( $\geq 90$ ; bovine), histone (type IIA from calf thymus), and deoxyribonucleic acid (DNA) (from human placenta) (Sigma, St. Louis, MO) were chosen as representative biochemical constituents of spinal tissue, to be used for regression analysis. These chemicals were selected because they most likely represent the principal constituents that give rise to prominent Raman spectral features seen in spinal tissue.

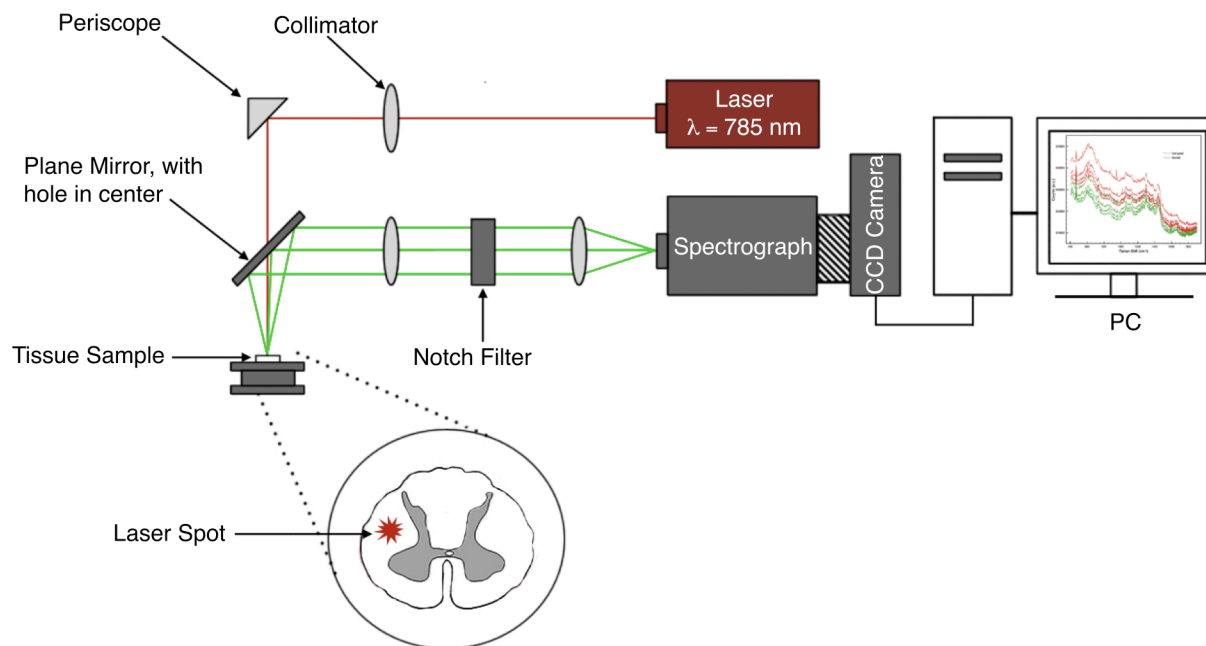


**Fig. 2** Schematic of the custom-built Raman spectroscope used in this study. Red lines represent excitation light, while green lines represent emissions. The zoomed-in area shows the normal incidence of the excitation light to the transverse plane of the tissue slice. Note that the laser spot position was not fixed amongst tests, although the spot was always constrained to the white matter.

Certain chemicals were chosen for their unique spectral characteristics, while others were chosen as general representations of their class of biomolecule. For example, triolein, a symmetrical triglyceride, was chosen as a representation of typical lipid vibrational modes, such as CH<sub>2</sub> twisting and bending. All constituents, with the exception of triolein, which was purchased in solution, were purchased and analyzed as lyophilized powders. Powders were placed in a cylindrical quartz cuvette, and triolein was placed in a custom borosilicate glass tube with stopper. Each spectrum was collected as 1,200 accumulations of 1.0-second integrations (total time of 20 minutes), and a minimum of 3 spectra were collected for each constituent. Spectra from the 11 biochemical species were used for regression analysis.

### *3.7 Spectroscopic data analysis*

Spectroscopic data sets were analyzed using MATLAB (Release 2011a; The Mathworks Inc., Natick, MA). Spectra were cropped to the finger print region of organic molecules ( $400\text{ cm}^{-1}$  to  $1800\text{ cm}^{-1}$ ) and baseline corrected using the 'msbackadj' function in MATLAB. For each spectrum, the 'msbackadj' function estimated a baseline within multiple shifted windows (of  $200\text{ cm}^{-1}$  width) and regressed the baseline using spline approximation before subtracting it from the spectrum. In this way, all Raman features narrower than  $200\text{ cm}^{-1}$  are preserved, while those wider are considered a product of background fluorescence and therefore removed. Because the tissue slices were sufficiently thin, emissions from the underlying PTFE membrane were collected coincidentally with tissue emissions, causing PTFE spectral features to appear within the tissue spectra. To correct for unwanted PTFE spectral features, an averaged PTFE membrane spectrum was subtracted from all tissue spectra. Subtraction was not performed on biochemical constituent spectra. Spectra were then smoothed using the 'mssgolay' function in MATLAB, which applied a Savitzky-Golay smoothing filter. Standardization was performed by mean centering the data and dividing by the standard deviation, i.e. standard normal variable (SNV) transformation. For qualitative assessment, a numerical value was assigned to 10 peaks of interest present within the tissue spectra using the 'findpeaks' function in MATLAB.

### *3.8 Modeling of spectroscopic data*

A semi-quantitative linear model of the spinal tissue spectra was rendered using partial least squares (PLS) regression. The PLS regression was performed in MATLAB (Release 2011a; The Mathworks Inc., Natick, MA) using a modified version of the

'plsregress' function. PLS regression was chosen for its ability to handle multicollinearity amongst predictor variables. The Raman spectra of biochemicals of a similar nature often share characteristic peaks, giving rise to a degree of correlation and hence necessitating the need for a regression technique capable of managing multicollinearity.<sup>26</sup> Such was the case for the biochemical constituents chosen for this model (See *Raman spectroscopy of biochemical constituents*). The goal of the PLS regression model was to describe the commonality between the spectra of spinal tissue and the spectra of the 11 reference biochemical constituents. To this end, we extracted, from the regression, the relative contribution of each biochemical constituent spectrum to each spinal tissue spectrum. Then, using the relative contributions, we tracked fluctuations in each biochemical over the course of the *in vitro* SCI and cABC treatment timeframe. The basic form of the PLS regression model is given by:

$$Y = X\beta + R \quad (1)$$

Where Y is an n-by-m response matrix, X is an n-by-p predictor matrix,  $\beta$  is a p-by-m matrix of linear coefficients, and R is an n-by-m matrix of response residuals. For this study, Y corresponds to an n-by-m matrix composed of the tissue spectra for a particular group (e.g SCI at 1 DPI), where n is the number of spectral intensity observations and m is the number of spectra; X corresponds to an n-by-p matrix composed of the mean constituent spectra, where p is the number of constituents; and  $\beta$  corresponds to a p-by-m matrix composed of the relative contributions of each constituent. PLS regression is a multivariate technique that operates by projecting predictor and response variables (i.e. X and Y) to a new space. X and Y are

simultaneously decomposed to find eigenvectors that explain a maximum amount of the covariance between X and Y. The projections of X and Y are given by:

$$X = X_S X_L^T + X_R \quad (2)$$

$$Y = Y_S Y_L^T + Y_R \quad (3)$$

Where  $X_S$  and  $Y_S$  are n-by-ncomp score matrices, with ncomp equal to the number of allowed PLS components. For this study, ncomp is equal to the total number of constituents so that ncomp equals p. The columns of  $X_S$  and  $Y_S$  are the eigenvectors. X and Y are regressed onto Xs to find the predictor and response loading matrices,  $X_L$  and  $Y_L$  respectively.  $X_L$  is a p-by-ncomp matrix of predictor loadings, with row values corresponding to coefficients that estimate the original predictor variables; and  $Y_L$  is an m-by-ncomp matrix of response loadings, with row values corresponding to coefficients that estimate the original response variables.  $X_R$  and  $Y_R$  are matrices that contain the residual from each projection. The linear coefficient matrix,  $\beta$ , can be given in terms of the response and predictor loading matrices as follows:

$$\beta = Y_L^T (X_L^T)^{-1} \quad (4)$$

$\beta$  provides linear coefficients that represent the relative contribution of each predictor variable, or constituent, on the response matrix. However, PLS regression may yield negative coefficients in  $\beta$ , which as contributions have no physical meaning. To eliminate negative values, the 'plsregress' function in MATLAB was modified to enforce a non-negativity constraint by replacing its original decomposition method of singular value decomposition (SVD) with non-negative matrix factorization (NNMF). NNMF

was accomplished using the built-in 'nnmf' function. Rows in  $\beta$  were averaged to produce a mean linear coefficient for each constituent. Please recall that prior to regression, all spectra were SNV transformed to a mean of 0 and a standard deviation of 1; this produced standardized coefficients. For simplicity's sake, the 7 constituents with the largest standardized linear coefficients, and thus the largest relative contribution to the tissue spectra, were selected for further analysis and discussion; they are triolein, actin, cholesterol, collagen type IV, CS-C, histone, and DNA. To assess the progression of SCI and its treatment with cABC, relative contributions were found using PLS regression for SCI groups (n=18) and CTL groups (n=9) at 1, 4, and 8 DPI; and for SCI+cABC groups (n=18) and SCI+Sham groups (n=9) at 4 and 8 DPI. The variable 'n' refers to the number of measured spectra.

### *3.9 Statistical analysis*

Statistical analysis was performed using MATLAB (Release 2011a; The Mathworks Inc., Natick, MA). Data are given as mean  $\pm$  standard deviation (SD). All data, excluding that of SCI+cABC and SCI+Sham groups, were analyzed using one-way or two-way ANOVA as appropriate, followed by a post-hoc Tukey's HSD test. Comparison between SCI+cABC and SCI+Sham groups was conducted using an unpaired Student's t-test. For all tests, significance was assessed at  $p < 0.05$ .

## **4 RESULTS**

### *4.1 Viability of organotypic cultures*

Organotypic spinal cord slices were successfully cultured for up to 14 DIV using the interface method. Gross tissue morphology was visually inspected under microscopic



assistance once per day while in culture. We observed no discernable changes in the cross-sectional shape of the spinal cord over 14 DIV. Grey matter and white matter were easily distinguishable by visual examination, and both maintained their original shape and coloration. No degeneration or migration of the spinal horns or columns was seen. In most slices, a time-dependent flattening was observed, wherein tissue migrated outward from its original position, decreasing the height of the slice. Cell death significantly decreased following 1 DPI ( $p < 0.05$ , Tukey's HSD test) [Fig. 3(a)], which may indicate *in vitro* healing of the spinal tissue in response to excision and sectioning. There was no statistically significant difference between groups at 4, 7, 10, and 14 DIV, suggesting stability of cell death from 4 DIV to 14 DIV. The cell death averages for the aforementioned groups remained below a value of 12%. To ensure all cultures were stabilized prior to experimentation, a period of 6 DIV was allowed before the induction of SCI, as previously seen.<sup>27</sup>

#### 4.2 Cell death in response to SCI

To induce SCI, a stainless steel weight was dropped from a fixed height onto the center of the spinal cord slice. Gross tissue morphology was visually inspected at 1, 4, and 8 DPI. Starting at 4 DPI, we observed a slight curling of the slice edges away from the culture insert membrane, which indicates a loss of cell or extracellular matrix adhesion at the periphery. However, no changes in structure, location, or coloration of the white and grey matter were observed. A PI fluorescence assay was used to assess cell death at 1, 4, and 8 DPI. Compared to their controls, injured slices at each DPI time point demonstrated significantly increased cell death ( $p < 0.05$ , Tukey's HSD test): 1 DPI ( $12.3 \pm 4.1$  vs.  $7.9 \pm 1.9\%$ ), 4 DPI ( $26.7 \pm 5.9$  vs.  $7.7 \pm 2.1\%$ ), and 8 DPI ( $35.2 \pm 7.5$  vs.

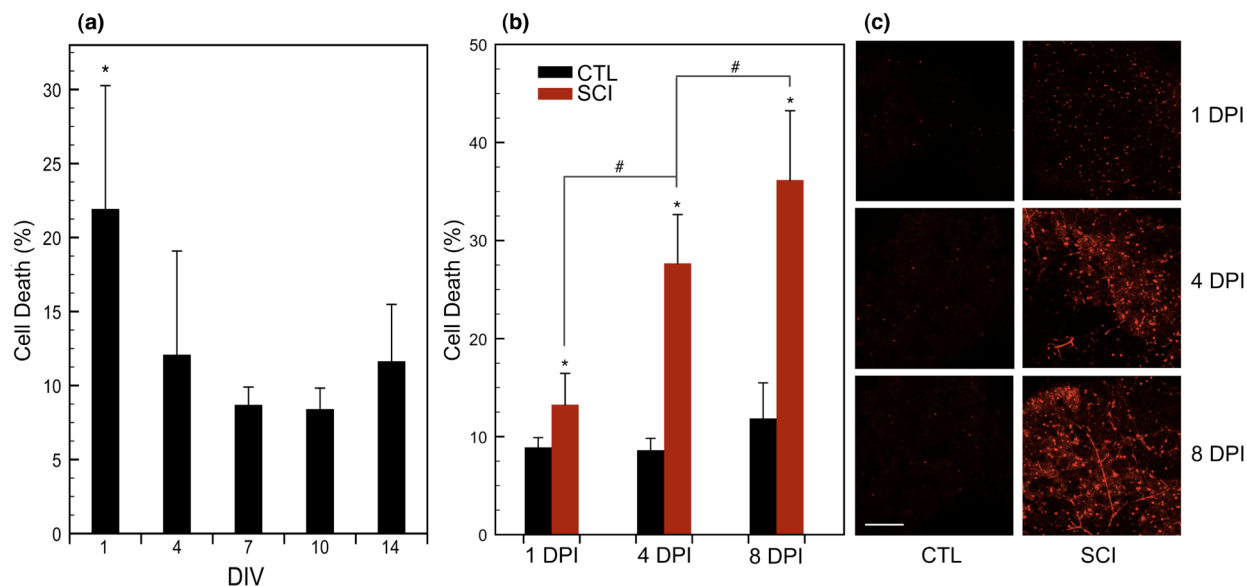


**Fig. 3** (a) Bar chart showing the percentage of cell death for uninjured spinal tissue cultures at varying DIV. Cell death decreases after 1 DIV and remains static at least until 14 DIV. Percentage of cell death was determined as described in Materials and Methods, and data are expressed as mean + SD. Statistical significance was determined using one-way ANOVA followed by a post-hoc Tukey's HSD test. Significance was assessed at  $p < 0.05$  and is denoted by an asterisk \*. (b) Percentage of cell death for SCI groups at varying DPI. CTL groups are uninjured. All SCI groups show a significant increase in cell death relative to controls. Statistical significance was determined using two-way ANOVA followed by a post-hoc Tukey's HSD test and was assessed at  $p < 0.05$ . An asterisk denotes significance between SCI and CTL groups, while # denotes significance between SCI groups only. (c) Representative micrographs (10X) of PI staining. Scale bar=200  $\mu\text{m}$  and is applicable to all micrographs. Noticeable increases in fluorescence are demonstrated for all groups.

10.9 $\pm$ 4.5%) [Fig. 3(b)]. Additionally, injured slices demonstrated a monotonic increase in cell death over time ( $p < 0.05$ , Tukey's HSD test) (12.3 $\pm$ 4.1% @1 DPI, 26.7 $\pm$ 5.9% @4 DPI, 35.2 $\pm$ 7.5% @8 DPI). Two-way ANOVA suggests there is a synergistic effect of time and injury on the severity of cell death (interaction  $p$ -value=5.18E-09).

### 4.3 Raman Assignments

Raman spectra of spinal cord slice cultures were collected as previously described. Prominent Raman bands were labeled with a peak wavenumber value and assigned to a vibrational group/mode (Table 1). Vibrational groups were then assigned to a probable biochemical based on biological relevance to spinal tissue.

**Table 1** Band assignments for spinal tissue spectra. Greek letters denote the type of vibrational mode ( $\nu$ =stretching,  $\nu_s$ =symmetric stretching,  $\delta$ =bending) and qualifiers denote the specific type of stretch/bend. Reference numbers refer to the assignment's source.

Peak Wavenumber (cm <sup>-1</sup> )	Vibrational Group/Mode	Biochemical Assignment	Reference Number
540	C-OH	Saccharides	28
643	$\delta$ (C-C) twisting, C-S	Tyrosine	29, 30, 31
700	Sterol ring	Cholesterol	17, 32
890	C <sub>(1)</sub> -H	$\beta$ -anomers	28, 33, 34
913	C-OH	Saccharides	28, 35
1003	$\nu_s$ (C-C) breathing	Phenylalanine	30, 33
1064	$\nu$ (C-C) stretching	Lipids	28, 31, 33
1137	C-H, C-OH	Saccharides	16
1300	$\delta$ (CH <sub>2</sub> ) twisting	Lipids	31, 32, 35
1445	$\delta$ (CH <sub>2</sub> ) bending/scissoring	Lipids	30-32
1660	Amide I / $\nu$ (C=O) stretching	Proteins / lipids	30-32

#### *4.4 Culturing has a negligible effect on the Raman spectra of organotypic spinal tissue*

To study the effect culturing has on the Raman features of spinal tissue, spectra were collected for cultured slices at 7, 10, and 14 DIV. As a control, spectra were collected from uncultured slices immediately following the excision and slicing procedure. Figure 4A shows the mean, baseline-corrected, SNV transformed spectrum for each of the aforementioned groups. Spectra are stacked so that each spectrum is completely and easily discernable. In order to clearly see the variation between cultured and uncultured slices throughout the culture timeline, we provide difference spectra using the uncultured slice group as a reference [Fig. 4(b)]. Between-group comparison of peak intensity shows a statistically significant decrease at 700 cm<sup>-1</sup> (sterol ring of cholesterol) between 7DIV/ 10 DIV and uncultured slices ( $p < 0.05$ , Tukey's HSD test) (Table 2). There are no statistical differences at any remaining peaks. These results indicate a

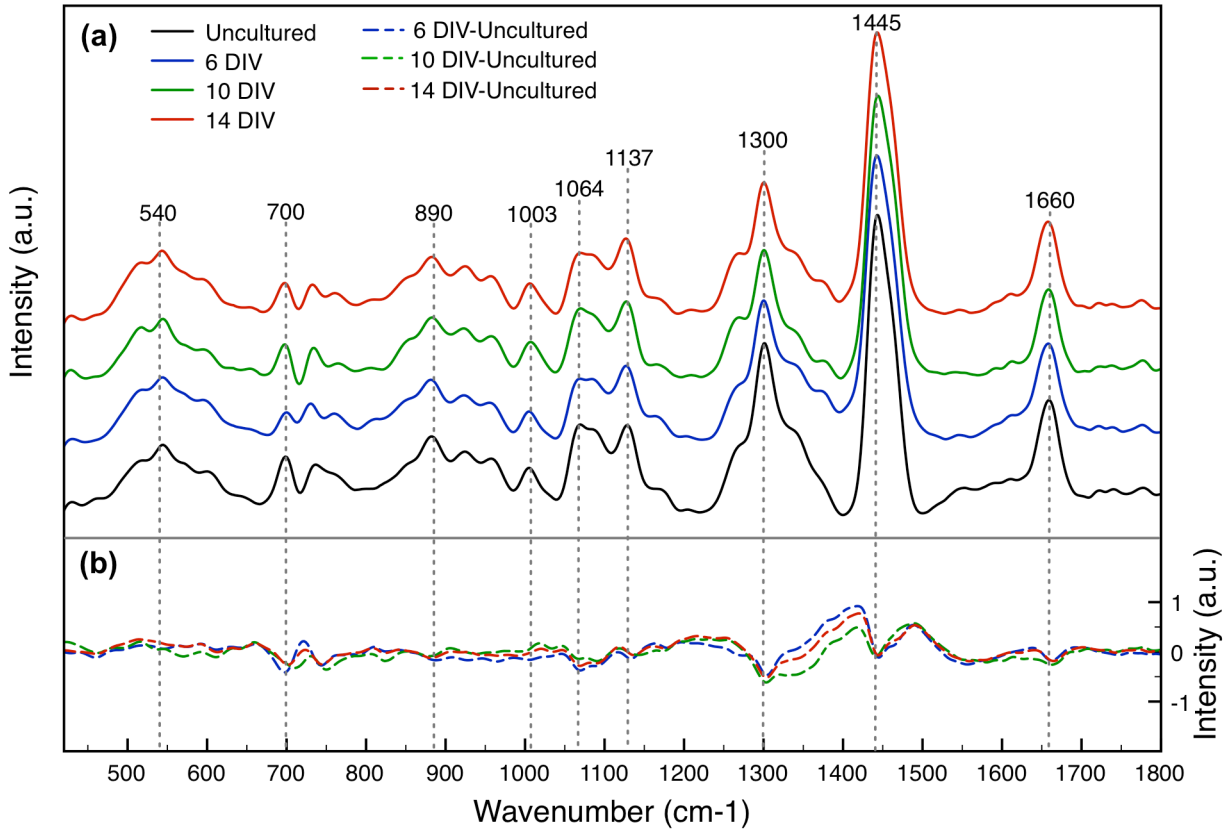


**Fig. 4** (a) The mean, baseline-corrected, SNV-transformed spectra of uninjured, cultured spinal tissue at 6, 10, and 14 DIV. An uncultured spinal tissue spectrum is presented for comparison. Spectra are stacked to clearly show features. (b) Difference spectra obtained using the uncultured spectrum as a reference. The goal was to visualize the effect time in culture has on tissue spectra. Note that difference spectra were generated before stacking, using zero-centered spectra.

**Table 2** Statistical comparison between peak intensities of uninjured groups at varying DIV, as determined by one-way ANOVA followed by a *post-hoc* Tukey's HSD test. Significant was assessed at  $p < 0.05$ . Groups with dissimilar letters are significantly different. Dashes (-) denote no statistical significance between any groups.

Peak Wavenumber (cm <sup>-1</sup> )	p-value	Uninjured Groups			
		Uncultured	6 DIV	10 DIV	14 DIV
540	0.3243	-	-	-	-
700	0.0078	A	B	B	A,B
890	0.1213	-	-	-	-
913	0.0765	-	-	-	-
1003	0.0796	-	-	-	-
1064	0.4445	-	-	-	-
1137	0.1786	-	-	-	-
1300	0.0519	-	-	-	-
1445	0.4305	-	-	-	-
1660	0.3895	-	-	-	-

possible drop in cholesterol concentration following initial incubation. Between 7 and 14 DIV, however, we can infer there are no significant changes in the biochemistry contributing to Raman spectral features. These data, in conjunction with data on cell death, suggest a period of quiescence during the tissue's second week in culture.

#### *4.5 Effect of SCI on the Raman spectra of organotypic spinal tissue*

To assess Raman spectral changes in response to SCI, spectra were collected for SCI groups at 1, 4, and 8 DPI. Spectra for uninjured CTL groups were collected at similar times. Figure 5(a) shows the mean, baseline-corrected, SNV transformed spectrum for SCI groups at 1, 4, and 8 DPI. Statistical comparison between peak intensities was performed using one-way ANOVA with a post-hoc Tukey's HSD test ( $p < 0.05$ ) (Table 3). For simplicity, only peaks of statistical significance are discussed. Note that a relative change in peak intensity is representative of a relative change in the concentration of a peak's assigned biochemical. Monotonic decreases in intensity were seen at  $1300\text{ cm}^{-1}$  [ $\delta(\text{CH}_2)$  twisting of lipids] and  $1445\text{ cm}^{-1}$  [ $\delta(\text{CH}_2)$  bending/scissoring of lipids]. These results suggest a time-dependent monotonic decrease in lipid concentration following SCI. Similar results have been observed using an *in vivo* model of SCI.<sup>16, 17</sup> The peak at  $700\text{ cm}^{-1}$  (sterol ring of cholesterol) decreased between 1 DPI and 4 DPI, and is visually absent from the spectrum at 8 DIV. Other notable decreases occurred at  $1064\text{ cm}^{-1}$  [ $\nu(\text{C}-\text{C})$  stretching of lipids] and  $1660\text{ cm}^{-1}$  [Amide I of proteins,  $\nu(\text{C}=\text{O})$  stretching of lipids] between 4 DPI and 8 DPI. Monotonic increases were observed at  $540\text{ cm}^{-1}$  (C-OH of saccharides) and  $913\text{ cm}^{-1}$  (C-OH of saccharides), with an additional increase at  $1137\text{ cm}^{-1}$  (C-H, C-OH of saccharides) between 4 DPI and 8 DPI. Interestingly, all increasing peaks are attributed to the deformation of C-OH. To further illustrate the

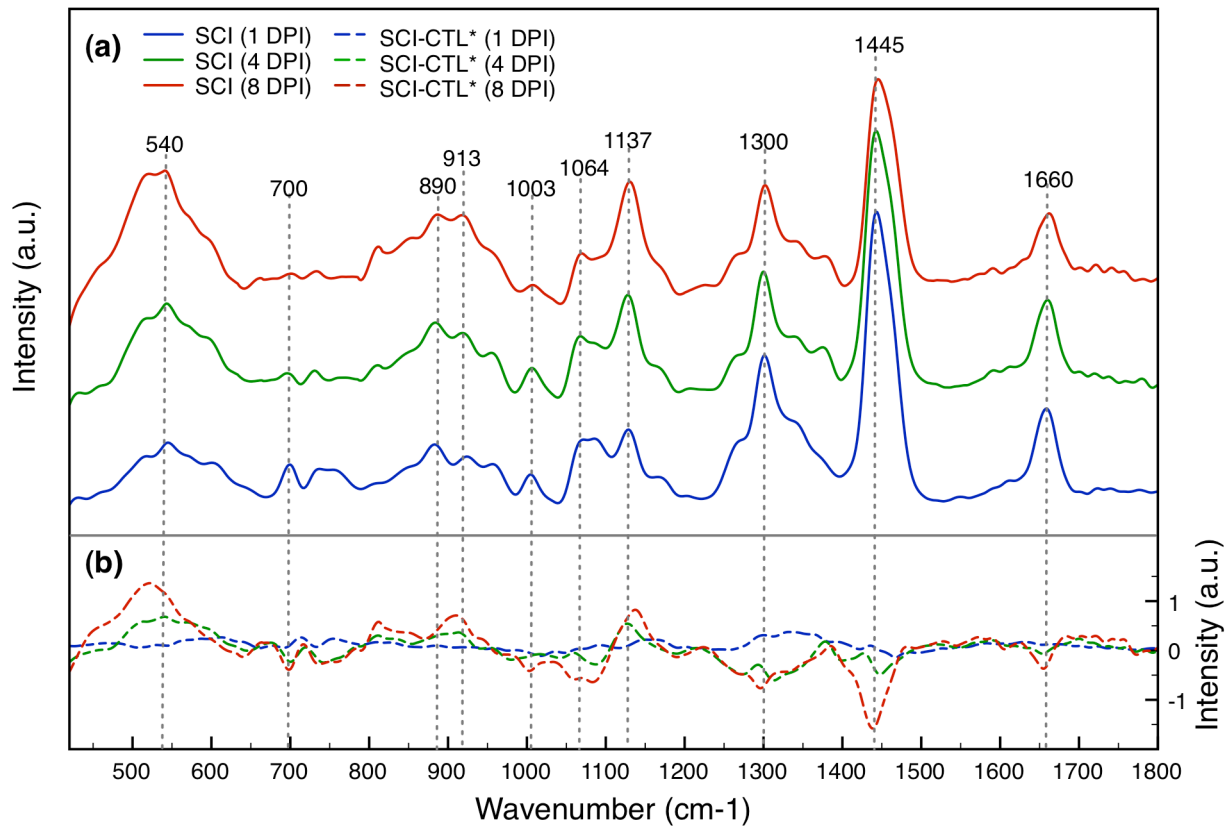


**Fig. 5** (a) The mean, baseline-corrected, SNV-transformed spectra of untreated, injured spinal tissue at 1, 4, and 8 DPI. Spectra are stacked to clearly show features. (b) Difference spectra obtained using uninjured control groups\* (at their respective DPI) as a reference. The goal was to visualize the progression of injury over time relative to the uninjured state. Note that difference spectra were generated before stacking, using zero-centered spectra.

**Table 3** Statistical comparison between peak intensities of SCI groups at varying DPI, as determined by one-way ANOVA followed by a *post-hoc* Tukey's HSD test. Significant was assessed at  $p < 0.05$ . Groups with dissimilar letters are significantly different.

Peak Wavenumber (cm <sup>-1</sup> )	p-value	SCI Groups		
		1 DPI	4 DPI	8 DPI
540	3.85E-08	A	B	C
700	2.55E-19	A	B	B
890	2.28E-04	A	A,B	B
913	1.94E-17	A	B	C
1003	1.69E-12	A	A	B
1064	8.29E-07	A	A	B
1137	6.41E-09	A	B	B
1300	9.95E-14	A	B	C
1445	2.06E-21	A	B	C
1660	2.66E-05	A	A	B

aforementioned spectral changes, difference spectra between SCI groups (1, 4, and 8 DPI) and their corresponding controls (Uninjured slices at 1, 4, and 8 DPI, respectively) are provided in Figure 5(b). The goal of the difference spectra is to visualize the progression of injury over time, relative to the uninjured tissue state.

#### *4.6 Effect of cABC treatment on the Raman spectra of injured organotypic spinal tissue*

Injured spinal cord slices were treated with cABC (0.2 U/ml) 1-hour post-injury and spectra were collected at 4 and 8 DPI. Figure 6 shows the mean, baseline-corrected, SNV transformed spectrum for cABC-treated groups (SCI+cABC) and sham-treated control groups (SCI+Sham) at 4 and 8 DPI. Statistical comparison between cABC and Sham-treated groups was performed using an unpaired Student's t-test, and significance was assessed at  $p < 0.05$  (Table 4). Compared to their control, cABC-treated slices showed significantly decreased intensity at  $540\text{ cm}^{-1}$  (C-OH of saccharides) ( $p = 7.61\text{E-}05$  for 4 DPI;  $p = 3.05\text{E-}03$  for 8 DPI) and at  $1137\text{ cm}^{-1}$  (C-H, C-OH of saccharides) ( $p = 1.06\text{E-}02$  for 4 DPI;  $p = 1.49\text{E-}02$  for 8 DPI), and significantly increased intensity at  $890\text{ cm}^{-1}$  [ $\text{C}_{(1)}\text{-H}$  of  $\beta$ -anomers] ( $p = 2.34\text{E-}02$  for 4 DPI;  $p = 2.39\text{E-}07$  for 8 DPI) and at  $643\text{ cm}^{-1}$  [ $\delta$ (C-C) twisting of proteins] ( $p = 2.56\text{E-}04$  for 4 DPI;  $p = 4.43\text{E-}02$  for 8 DPI). The peak at  $643\text{ cm}^{-1}$  is completely absent from the spectra of sham-treated slices, which suggests a sudden rise in a new vibrational mode, C-C twisting/C-S stretching, following cABC treatment. At 8 DPI only, cABC slices showed significantly increased intensity at  $1064\text{ cm}^{-1}$  [ $\nu$ (C-C) stretching of lipids] ( $p = 3.83\text{E-}04$ ). The intensity changes at  $540\text{ cm}^{-1}$ ,  $1064\text{ cm}^{-1}$ , and  $1137\text{ cm}^{-1}$  are antagonistic to those produced by SCI. Again to further illustrate the aforementioned spectral changes, difference spectra between cABC-treated groups and their sham-treated controls are provided in Figure 6.

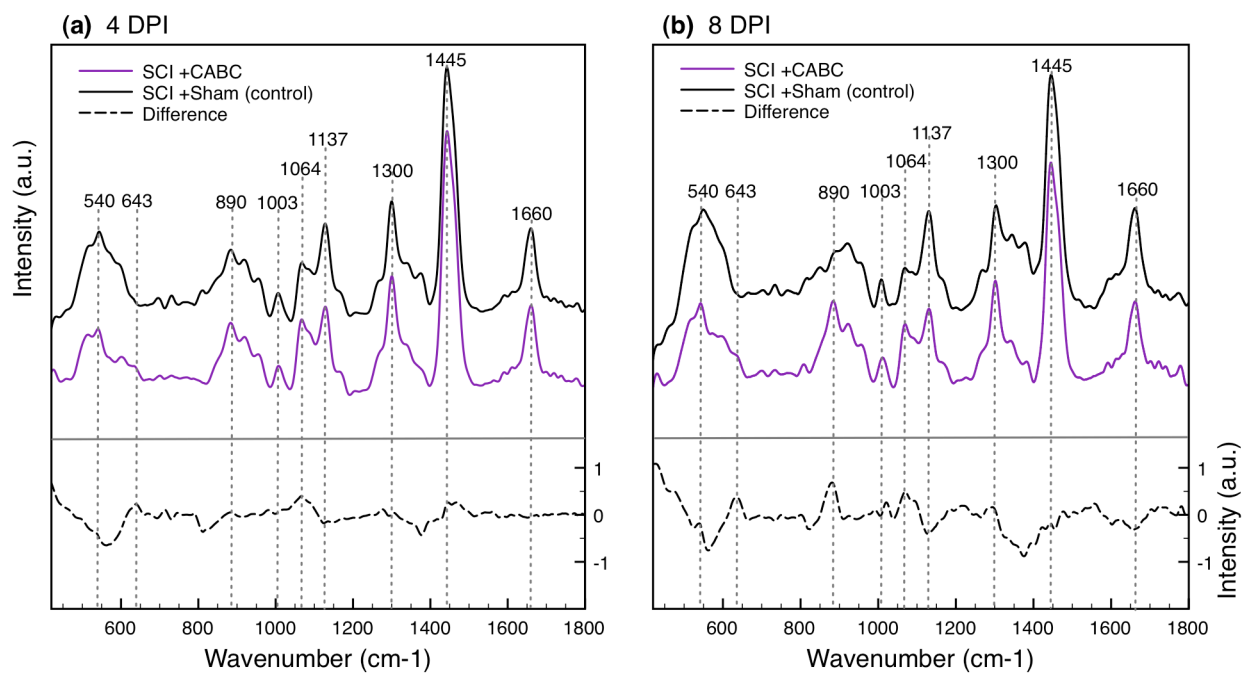


**Fig. 6** The mean, background corrected, SNV-transformed spectra of cABC-treated and sham-treated spinal tissue at (a) 4 DPI and (a) 8 DPI. Spectra are stacked to clearly show features. Note that difference spectra (cABC-Sham) were generated before stacking using zero-centered spectra.

**Table 4** Statistical comparison between peak intensities of cABC groups and their sham controls at varying DPI, as determined by an unpaired Student's t-test. For quick reference, asterisks indicate level of significance, \* $p < 0.05$ , \*\* $p < 0.01$ .

Peak Wavenumber ( $\text{cm}^{-1}$ )	<i>p</i> -value	
	cABC vs. Sham 4 DPI	cABC vs. Sham 8 DPI
540	**7.61E-05	**3.05E-03
643	**2.56E-04	*4.43E-02
700	5.11E-01	3.70E-01
890	*2.34E-02	**2.39E-07
913	6.63E-01	2.75E-01
1003	7.88E-01	9.29E-01
1064	8.41E-02	**3.82E-04
1137	*1.06E-02	*1.49E-02
1300	8.86E-01	6.60E-01
1445	5.37E-02	7.51E-01
1660	3.42E-01	2.52E-01



#### *4.7 Success of PLS regression model*

Table 5 shows the percentage of variance explained in Y (matrix of response variables, see Equation 1) by the PLS regression for each modeled group. Explained variance ( $\eta^2$ ) serves as an index of goodness of fit and is analogous to the coefficient of determination ( $R^2$ ), typically used in multiple regression models. Values for  $\eta^2$  range from 63.66 to 84.68%. We can see from the response residual, taken as the difference between the fitted response and the average measured tissue spectrum, that a large portion of unexplained variance comes from the 540  $\text{cm}^{-1}$  band and 1064  $\text{cm}^{-1}$  band (Fig. 7). This is especially true of SCI groups assessed later in culture, e.g. 8 DPI, as these bands increase significantly over the course of injury. However, despite the presence of weaker intensity bands in the fitted response, the PLS regression model is capable of largely resolving the response variance. Figure 8 shows the mean, baseline-corrected, SNV transformed spectrum for each of the 7 constituents chosen for discussion. These spectra were chosen for their higher standardized linear coefficient values, and offer the largest contribution amongst predictor variables to the PLS fitted response.

#### *4.8 Biochemical variations in response to SCI and cABC treatment*

PLS regression was used to ascertain the relative contribution of spectra from 11 predetermined biochemical constituents to the spectra of cultured spinal tissue. As previously mentioned, the regression model output standardized linear coefficients for each constituent, which, for the purposes of discussion, will be referred to as a constituent's relative contribution. Two models were constructed: the first for SCI groups and their uninjured controls, and the second for SCI+cABC groups and their

**Table 5.** Percent variance explained by PLS regression for each modeled group

Group	Variance explained by model (%)
Uninjured CTL (1 DPI)	83.39
SCI (1 DPI)	84.68
SCI (4 DPI)	75.53
SCI +cABC (4 DPI)	80.48
SCI +Sham (4 DPI)	77.35
SCI (8 DPI)	63.66
SCI +cABC (8 DPI)	71.87
SCI +Sham (8 DPI)	69.61

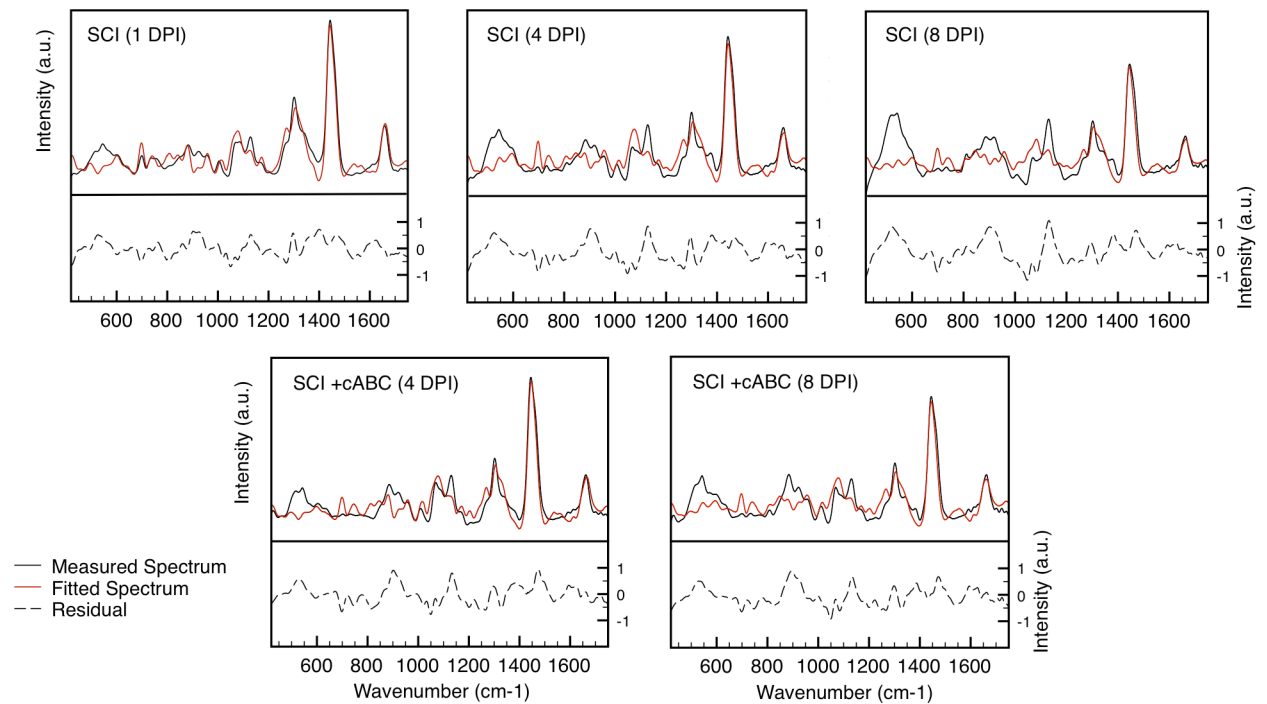


**Fig. 7** Measured spinal tissue spectra versus the fitted responses generated by PLS regression. For simplicity control groups are not shown. Residual is the difference between measured and fitted.

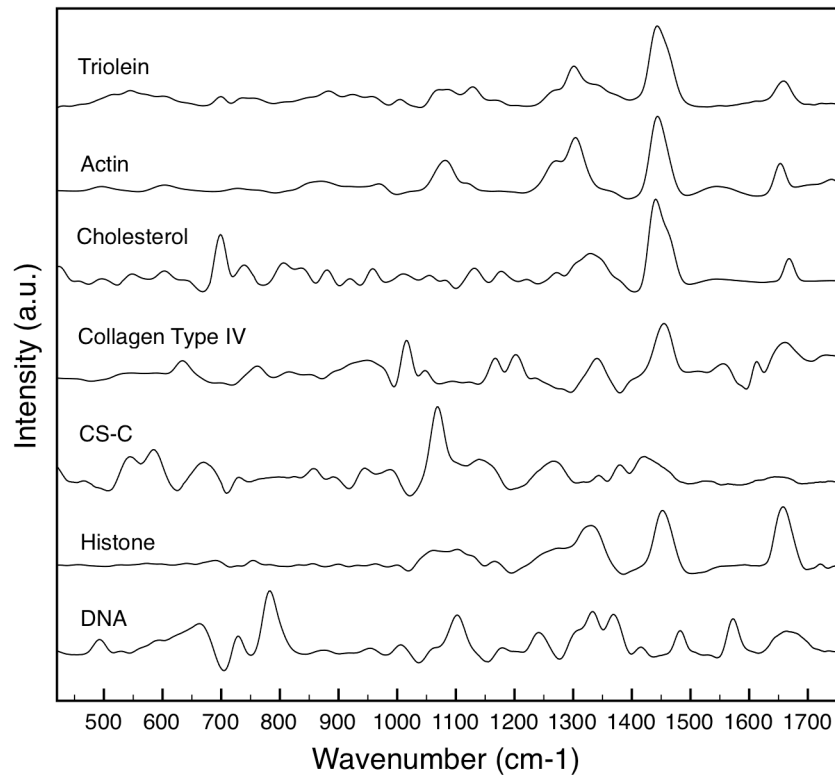


**Fig. 8** The mean, baseline-corrected, SNV-transformed spectra of the 7 biochemical species used for regression modeling. Spectra are stacked to clearly show features.

sham-treated controls. Figure 9 depicts the relative contribution of the 7 constituents (chosen for discussion) for SCI groups at 1, 4, and 8 DPI. For simplification, a single CTL group was chosen for comparison. Since we observed no significant spectral differences between CTL groups at 1, 4, and 8 DPI (results not shown), the CTL group at 1 DPI was chosen arbitrarily to serve this purpose. Data are shown as mean  $\pm$  SD, and between-group comparison was performed using a post-hoc Tukey's HSD test ( $p < 0.05$ ). A notable increase in relative contribution was observed for CS-C following 1 DPI; and notable decreases were observed for triolein, histone, and DNA following 1 DPI, and for cholesterol following 4 DPI. Figure 10 depicts the relative contributions for cABC-treated and sham-treated groups at 4 DPI and 8 DPI. Here sham-treated groups are controls. Between-group comparison was performed using an unpaired Student's t-

test, and significance was assessed at  $p < 0.05$ . At 4 DPI, a significant increase in relative contribution, relative to the control, was observed for collagen type IV, while significant decreases were observed for cholesterol and CS-C. Similarly, at 8 DPI, a significant increase was observed for collagen type IV, while significant decreases were observed for cholesterol and CS-C.

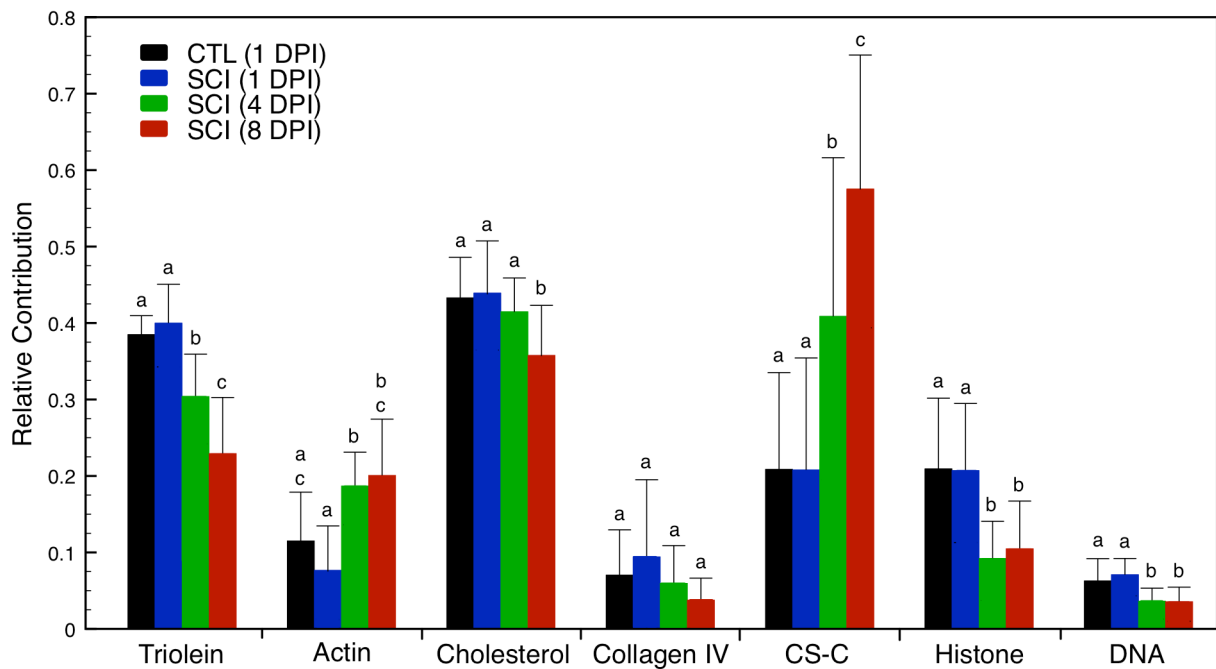


**Fig. 9** Bar chart displaying the relative spectral contributions of biochemical species to injured spinal tissue at 1, 4, and 8 DPI. A single uninjured CTL group was chosen for comparison. Note that relative contribution values are unitless, as they are synonymous to standardized regression coefficients. Data are expressed as mean + SD. Statistical significance was determined using one-way ANOVA followed by a *post-hoc* Tukey's HSD test. Significance was assessed at  $p < 0.05$  and groups with dissimilar letters are significantly different.

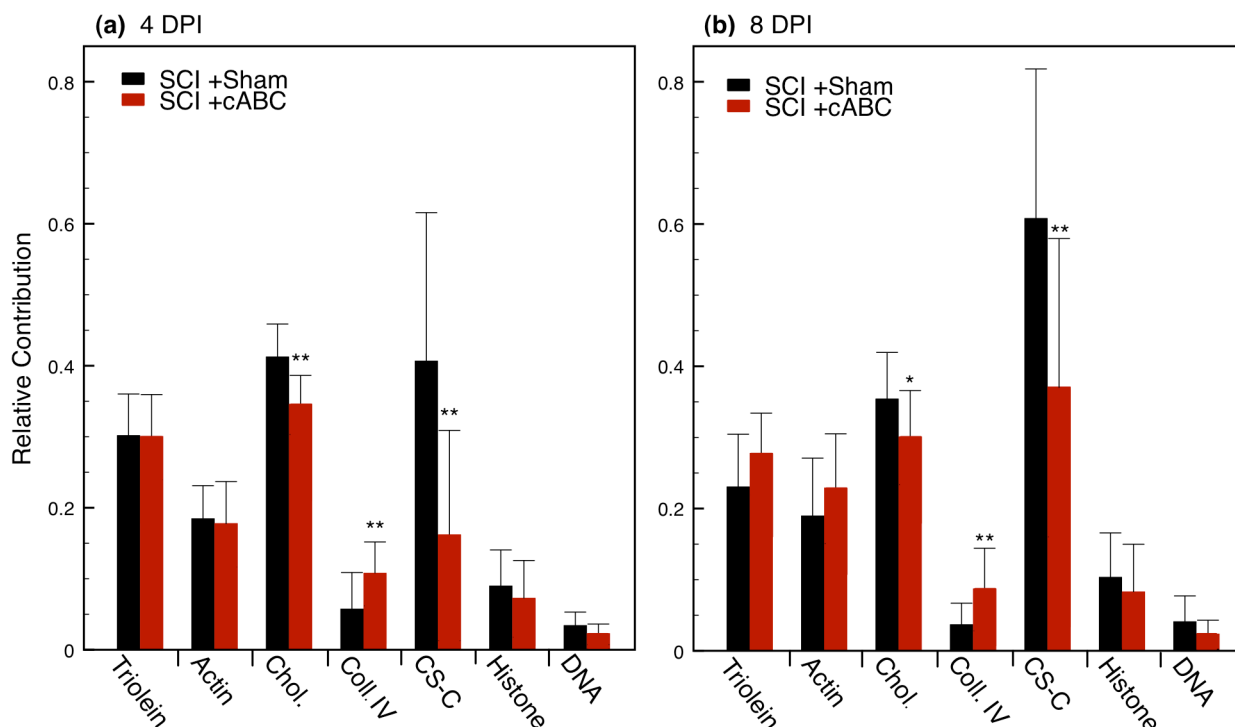


**Fig. 10** Bar chart displaying the relative spectral contributions of biochemical species to cABC-treated and sham-treated spinal tissue at (a) 4 DPI and (b) 8 DPI. Note that relative contribution values are unitless, as they are synonymous to standardized regression coefficients. Data are expressed as mean + SD. Statistical significance was determined using an unpaired Student's t-test. Asterisks indicate levels of significance, \*  $p < 0.05$ , \*\*  $p < 0.01$ .

## 5 DISCUSSION

Raman spectroscopy is a powerful tool in examining compositional and conformational phenomena in living tissue. As mentioned, its success is demonstrated in the qualitative assessment of spinal cord tissue. However, no reports to date have used Raman spectroscopy to examine the effects of enzymatic treatment on SCI. This study presents a novel spectroscopic investigation, in qualitative and semi-quantitative nature, of SCI and its treatment with cABC in an organotypic model.

Firstly, we generated a spectroscopic characterization of organotypic SCI using Raman spectroscopy. This allowed us to observe, from a spectroscopic perspective, which pathological events of SCI, if any, were functional in an organotypic setting.

We demonstrate that data in the present study exhibit strong agreement with previously established models of *in vivo* SCI<sup>16, 17</sup>; however, there are several developments that warrant discussion. Please note that the following discussion refers to significant differences between SCI groups and uninjured control groups, and that references for Raman assignments are listed in Table 1.

Relative to uninjured tissue, we observed a monotonic decrease in peak intensity for bands at 1445 cm<sup>-1</sup> and 1300 cm<sup>-1</sup>, over the timeframe of SCI. Both bands are attributed to CH<sub>2</sub> bending in lipids, so accordingly their decrease in intensity likely correlates to a decrease in lipid concentration. This is because, under constant test conditions, spectral intensity (at a particular frequency) is assumed proportional to the concentration of whichever Raman-active chemical is vibrating at that frequency.<sup>16</sup> Since all tissue samples were maintained *in vitro*, a reduction in concentration implies either a degradation of the chemical, or its secretion from the tissue matrix. Reduction in lipid concentration is concurrent with demyelination, a hallmark feature of the glial scar, wherein axons are stripped of their myelin coating.<sup>8,9</sup> Since myelin is largely composed of lipid molecules, a mass removal would likely reduce CH<sub>2</sub> vibrational modes, and thus decrease correlated band intensities.

Monotonic increases in peak intensity were observed at 540 cm<sup>-1</sup> and 913 cm<sup>-1</sup>, both of which are attributed to C-OH deformation. For either band, the C-OH group is assigned to saccharides. Applicably, the 540 cm<sup>-1</sup> band was observed in the spectra of aggrecan, a type of CSPG, and more specifically in the spectra of chondroitin sulfate-A and chondroitin sulfate-C, the unbranched polysaccharide side-chains of CSPGs.<sup>36</sup> This report<sup>36</sup> demonstrates an increase in intensity at 540 cm<sup>-1</sup> during CSPG aggregation, a

well-documented event of the glial scar<sup>1,11-14,16</sup>, suggesting that our observation may be more specifically, and perhaps more appropriately, assigned to CSPGs. This additional assignment stands to reason, if only because CSPGs are a major Raman-active component of injured spinal tissue's extracellular matrix<sup>16</sup>, and would therefore produce a significant spectral contribution. It should be noted that Raman spectroscopy is typically incapable of detecting chemicals of a concentration less than one part per thousand; so presumably, only chemicals of relatively high concentration within spinal tissue can produce observable spectral phenomena. If the assignment were hypothesized correctly, the increase at 540 cm<sup>-1</sup> would correlate to an upregulation of CSPGs, which is in agreement with SCI characteristics. The 913 cm<sup>-1</sup> band has been observed in monosaccharides, such as glucose and ribose<sup>35</sup>; however, intriguingly is not found in the spectra of chondroitin sulfate, a chain of alternating monosaccharides that contains glucuronic acid, which is structurally similar to glucose. Nevertheless, the increase at 913 cm<sup>-1</sup> suggests an increase in saccharide concentration following injury, which may also correlate to the upregulation of CSPGs.

In all observed tissue spectra, the peak at 913 cm<sup>-1</sup> overlaps with neighboring bands occupying the region from 800 cm<sup>-1</sup> to 970 cm<sup>-1</sup>. Bands in this region are largely attributed to C-O-C deformation seen in the glycosidic linkages of oligo- and polysaccharides.<sup>37</sup> We observed a monotonic increase in intensity over this entire region, which suggests the presence of newly formed glycosidic linkages. This is concurrent with CS-GAG polymerization during CSPG upregulation.

Overall, these spectral phenomena are grossly concurrent with *in vivo* SCI, in that they suggest demyelination and CSPG upregulation, two major hallmarks of the

glial scar. Prior models of *in vivo* SCI demonstrate similar occurrences at 1445, 1300, and 700  $\text{cm}^{-1}$ <sup>16,17</sup>; in the regions of 850-1000  $\text{cm}^{-1}$ <sup>16,17</sup>; and below 600  $\text{cm}^{-1}$ <sup>16</sup>. This last occurrence was not unanimous, but perhaps only because wavenumbers below 600  $\text{cm}^{-1}$  were left unobserved. Histological staining for myelin and immunohistochemical staining for chondroitin sulfate (types A and C) were used as references for spectral observations in the former study.<sup>16</sup> Said staining revealed a decrease in myelin levels as early as 4 DPI, and an increase in chondroitin sulfate levels, also as early as 4 DPI. These results, while not conclusive in their correlation to spectral observations, serve as positive evidence for their spectral hypotheses, and by extension our spectral hypotheses, regarding CSPG and myelin variations.

Secondly and subsequent to *in vitro* SCI, spinal tissue cultures were treated with cABC, a bacterial enzyme shown to attenuate the inhibitory properties of the glial scar. We demonstrate several key differences between the Raman spectra of cABC-treated spinal tissue and their sham-treated controls. This is significant for two reasons. First, it demonstrates that enzymatic treatment of SCI may be assessed spectroscopically. Second, it allows us to use the spectral differences to elucidate previously unknown mechanisms involved in the enzymatic reaction of cABC on injured spinal tissue. Unless stated otherwise, the following differences were observed between cABC-treated groups and sham-treated control groups at both collection times (4 and 8 DPI), and are statistically significant.

The most notable difference, relative to the sham control, was a decrease in peak intensity at 540  $\text{cm}^{-1}$ . This change is antagonistic to the injury response and, based on our previous assignment for this band, would suggest a decrease in CSPG



concentration. Reduced CSPG concentration is in agreement with the characterized action of cABC since the enzyme degrades the CS-GAG chains of CSPG<sup>1</sup>, rendering its original chemical structure forfeit. Furthermore, this result fine-tunes the 540 cm<sup>-1</sup> chemical assignment from CSPG as a whole to, more specifically, its CS-GAG chains. This is because cABC only interacts with the saccharide chains of CSPGs and not the protein core<sup>38</sup>, so any spectral variations produced by cABC are firstly assumed a result of the enzyme-substrate interaction.

We observed another notable decrease in peak intensity at 1137 cm<sup>-1</sup>. This band is attributed to C-H and C-OH deformation, and assigned to saccharides, suggesting a reduction in saccharide concentration post-treatment. If correctly assigned, this indicates depolymerized saccharides are eliminated from the extracellular matrix following the cABC enzymatic reaction. However, we cannot postulate a more direct correlation between the 1137 cm<sup>-1</sup> band and cABC treatment, as the band has not been strongly observed in the spectrum of cABC or its substrate, chondroitin sulfate (see Figure 8 for CS-C spectrum).

We observed an increase in peak intensity at 890 cm<sup>-1</sup>, which bears a specific assignment to  $\beta$ -anomers.  $\beta$ -anomers are cyclic saccharides that have a trans configuration between the OH group on C<sub>(1)</sub>, also referred to as the anomeric carbon, and the CH<sub>2</sub>OH<sub>2</sub> group on C<sub>(5)</sub>. The exact vibrational group(s) that give rise to this band are debated; although the band appears to be resultant of a combination of vibrations found in  $\beta$ -anomers, including CH<sub>2</sub>, C-O<sub>(5)</sub>, and C<sub>(1)</sub>-H deformations.<sup>35</sup> Several studies affirm C<sub>(1)</sub>-H deformation as the primary contributor.<sup>28, 33, 34</sup> Interestingly, CS-GAG chains are composed entirely of  $\beta$ -anomers, specifically glucuronic acid and

galactosamine. These two monosaccharides are repeatedly linked together by glycosidic linkages between the C<sub>(1)</sub> of one monosaccharide and the C<sub>(4)</sub> of another to form chondroitin sulfate. Raman spectral analysis of chondroitin sulfate reveals a strong appearance of the band in the spectra of chondroitin-6-sulfate (CS-C) and a medium appearance in that of chondroitin-4-sulfate (CS-A).<sup>36</sup> This data, along with details regarding the high extracellular concentrations of CSPGs during SCI<sup>39</sup>, suggests that our observation in spinal tissue may be more specifically assigned to chondroitin sulfate. Yet, while this information helps elucidate the source of spectral activity, it does not convey the reason for an increase in intensity. Any correlation between cABC treatment and increased  $\beta$ -anomer deformation is not apparent in the literature. However, we can speculate a cause. Studies have shown that cABC enzymatically degrades CS-GAG chains by cleaving the glycosidic linkages between its saccharide subunits<sup>40</sup>, which would directly affect the behavior of C<sub>(1)</sub>, as it is an integral part of the linkage. Thus, cleavage of the linkage may increase deformation in C<sub>(1)</sub>-H, perhaps by alleviating vibrational hindrances caused by surrounding functional groups of the CS-GAG chain.

A distinctive band at 643 cm<sup>-1</sup> was observed in the spectra of cABC-treated tissue, but not in sham-treated controls. Vibrations at 643 cm<sup>-1</sup> have two common assignments in the literature: the C-C twisting mode in tyrosine<sup>29,31</sup>, specifically within the phenol side-group, and the C-S stretching mode in sulfotyrosine.<sup>30</sup> Because of the ambiguity in assignment for this band, we offer two possible explanations for its occurrence. First, if we assume the band is correctly assigned to C-S stretching in sulfotyrosine, its occurrence is likely an outcome of protein tyrosine sulfation, a post-translational modification that is carried out on a variety of secreted and intra-membrane

proteins.<sup>41</sup> Protein tyrosine sulfation largely serves to strengthen, and thereby control, the interaction between secreted proteins and pathogens during the innate immune response.<sup>41</sup> Treatment by the bacterial-derived cABC has been known to invoke an immune response<sup>10</sup>, and even in the extrinsically restricted environment of organotypic culture, spinal tissue is capable of producing an innate immune response without the influences of systemic cells because of the presence of microglia.<sup>42</sup> If so, tyrosine sulfation would expectedly be a component of that response. Second, if the band is instead assigned to C-C stretching in tyrosine, its occurrence is likely due to conformational/compositional changes in protein structure. The spectral activity of the phenol side-group is highly sensitive to the orientation of its tyrosine residue<sup>29</sup>, so by affecting tyrosine orientation, it is feasible for a conformational/compositional change to increase intensity. This hypothesis is supplemented by a negative frequency shift from  $643\text{ cm}^{-1}$  to  $640\text{ cm}^{-1}$ , occurring between 4 and 8 DPI. The shift signifies a change in the stress/strain state of protein tyrosine, most likely caused by new vibrational groups surrounding protein tyrosine. Moreover, the shift signifies a continual conformational/compositional change to protein structure, one that evolves over the course of treatment. It is unclear exactly which proteins underwent changes, but we maintain CSPG core proteins as plausible candidates.

Lastly, we observed an increase in peak intensity at  $1064\text{ cm}^{-1}$  following 8 DPI. This band is attributed to C-C stretching in lipids. An increase in lipid concentration post-treatment, however subtle, may indicate remyelination facilitated by the action of cABC, whether it be on previously demyelinated or newly sprouted axons. Under normal SCI conditions, CSPGs inhibit remyelination by physically and chemically restricting

endogenous oligodendrocyte progenitor cells (OPCs) from differentiating and consequently attaching to bare axons.<sup>8</sup> During treatment, however, cABC overrides this inhibitory response on remyelination by enzymatically degrading CSPGs. With reduced CSPG action, OPCs are now free to myelinate. Intriguingly, this is the only significant difference that was not observed at both DPI. The lack of statistical difference between cABC-treated and sham-treated peaks at  $1064\text{ cm}^{-1}$ , and furthermore at  $1300\text{ cm}^{-1}$  and  $1445\text{ cm}^{-1}$  (all assigned to lipids), following 4 DPI, suggests that cABC-treated tissue did, in fact, undergo demyelination. Therefore any subsequent increase in lipid concentration may correlate to remyelination.

While comparing spectral intensities elucidates us to changes in concentration for biochemical species, it does so qualitatively and somewhat presumably, as it relies on tentative biochemical assignments. To help quantify the changes in biochemical species inherent in spinal tissue, we constructed two semi-quantitative linear models using PLS regression: one for SCI groups at varying DPI (1, 4, and 8 DPI), with uninjured controls, and another for cABC-treated groups at varying DPI (4 and 8 DPI), with sham-treated controls. For each biochemical constituent (chosen as a predictor variable), the PLS regression provides a standardized linear coefficient value that represents the constituent's relative contribution to the spinal tissue spectrum (chosen as the response variable). Note that the following discussion refers to significant between-group changes in relative contribution. A change in contribution indicates that more/less of a biochemical is observed in the spectra of spinal tissue, which implies a change in the biochemical's concentration.

From our regression model of SCI, we demonstrate that triolein and cholesterol monotonically decrease following injury. As previously stated, certain constituents were chosen for their unique spectral characteristics, while others were chosen as general representations of their class of biomolecule. Triolein and cholesterol were chosen as representation for typical lipid vibrational modes, such as CH<sub>2</sub> twisting and bending, often present in the region from 1300 cm<sup>-1</sup> to 1470 cm<sup>-1</sup>. A decrease in lipid contribution is concurrent with our spectral observations, and is indicative of demyelination. Histone and DNA were chosen as another such representation, albeit slightly different in nature. These constituents represent the characteristic vibrational modes contained within cell nuclei. We demonstrate a decrease in histone and DNA between 1 DPI and 4 DPI, with no further changes following 4 DPI. The results for histone are in agreement with other reports<sup>43,44</sup>, which demonstrate a release of histones from apoptotic cells during injury. From our results, we might further assume that histones are released from the extracellular matrix as well. Interestingly, the results for DNA are in disagreement with other reports that have spectroscopically characterized various pathologies.<sup>45, 46</sup> When DNA undergoes denaturation - a regular occurrence in apoptotic cells and one well characterized in CNS injury<sup>18</sup> - its secondary structure changes, which has a significant affect on its absorptivity.<sup>47, 48</sup> Reports demonstrate that the absorptivity change associated with DNA denaturation produces Raman hyperchromic effects<sup>47, 48</sup>, so one would assume the contribution of DNA to increase, rather than decrease, in response to injury. However, these findings may prove irrelevant, as they were conducted with an excitation source ranging below 300 nm (compared to ours of 785 nm). We maintain that the Raman hyperchromic effect may not be detectable for larger wavelengths; or

rather may not be detectable amongst the assortment of spectral activity in spinal tissue. CS-C differed most notably out of the seven constituents, increasing by the largest factor between 1 and 8 DPI. An increase in chondroitin sulfate concentration during the first week of injury is well documented<sup>39</sup>, and our results are in agreement.

From our regression model of cABC-treated SCI, we demonstrate a higher contribution from collagen type IV relative to sham-treated controls. Collagen type IV has not been previously characterized during cABC-treatment of SCI, so it is difficult to draw firm conclusions as to the cause of this result. However, one study reports that fibroblast-like cells present in the matrix of the annulus fibrosus, a component of the intervertebral disc, upregulate collagen in response to cABC treatment in an attempt to replenish the extracellular matrix of the disc.<sup>49</sup> They observed a significant increase in collagen concentration as early as 7 days after cABC treatment. While the study is merely analogous to spinal tissue treatment, it is certainly helpful in elucidating a supposition. From their work, we adopt the hypothesis that collagen synthesis in spinal tissue is activated by chemical or mechanical changes to the extracellular matrix following CSPG degradation. Studies demonstrate that collagen has its own axonal inhibitory properties, and that the collagen-rich basal membrane found in spinal tissue acts as a barrier to axonal regrowth.<sup>6,9</sup> So it is possible that cells upregulate collagen in an effort to restore or compensate for the inhibitory potential lost during cABC-treatment. This hypothesis implies that fibroblasts or fibroblast-like cells capable of synthesizing collagen, such as astrocytes, are present in the spinal tissue cultures. We demonstrate a lower contribution from cholesterol, relative to sham-controls, and no significant differences in triolein contribution. These data conflict with our initial spectra-derived

hypothesis of a decrease in lipid concentration following 8 DPI. This suggests one of two things. Either the  $1064\text{ cm}^{-1}$  band, which is the band that prompted the initial hypothesis, is incorrectly assigned to lipids or perhaps shares a latent assignment to another, more relevant molecule; or the model's explanation of variance within this spectral region is sufficiently low as to cause discrepancy between results. If the model were incapable of properly explaining variance in intensity at  $1064\text{ cm}^{-1}$ , then any changes in intensity, below a certain threshold, would be lost. A large residual around the  $1064\text{ cm}^{-1}$  band, relative to all other bands (see Fig. 7), lends credibility to the latter supposition. Lastly, we demonstrate a sizeable decrease in CS-C relative to sham-treated controls. At 8 DPI, CS-C contribution between cABC and sham-treated groups differs by the largest factor amongst constituents. A decrease in CS-C is in agreement with our spectral observations, as well as previous works<sup>1, 11-14</sup>, which demonstrate reduction in CS-GAGs concentration as early as 24 hours post-treatment.

## **6 CONCLUSION**

In conclusion, we demonstrate that Raman spectral variations characteristic of SCI can be observed using an organotypic model. These variations are hypothesized to correlate with demyelination, CSPG upregulation, and apoptosis, among other events within injured spinal tissue. This is significant in that it indicates prominent pathobiological events associated with *in vivo* SCI can be recapitulated *in vitro*, as far as spectral analysis is concerned, so that we have a functioning model of SCI. Moreover, we have a model of SCI that can be systematically treated and assessed within a controlled environment. To that effect, we demonstrate for the first time that Raman spectral variations are discernable during cABC treatment of SCI. Observed variations

are hypothesized to correlate with the enzymatic degradation of CS-GAGs, protein conformational/ compositional changes, and remyelination. PLS regression modeling confirms changes in lipid (presumably that of myelin) and CSPG concentration during SCI and its cABC treatment, and provides a semi-quantitative measure of these changes. Overall, these data establish Raman spectroscopy as a viable resource for monitoring the treatment of SCI with the enzyme, cABC. As a result, it is intriguing to consider the implications of Raman spectroscopy in up-and-coming chondroitinase-based SCI therapies.

## **7 FUTURE WORK**

The PLS regression produced an average explained variance of 75.82%, leaving marked room for improvement. We conceive three primary reasons for the unexplained variance. First, the PLS model operates on the assumption that the Raman spectra of a biochemical in isolation is identical to its Raman spectra once its been incorporated in tissue. If this assumption is broken, and the incorporation of a biochemical causes shifts in frequency, the model's ability to predict standardized coefficients could be adversely affected. Second, the set of predictor variables, i.e. biochemical constituents, chosen for this model may not have been optimal. If Raman bands found in the tissue are missing from the collection of reference spectra, the model will have a tendency to overfit certain predictor variables. This may have been the case for the  $1064\text{ cm}^{-1}$  band. To correct this issue, one might consider using a semi-parametric model that accounts for the omission of relevant predictor variables using a non-parametric term. However, a challenge presents itself in creating a semi-parametric model with non-negative restrictions. Third, the non-negativity constraint on the regression may have increased



unexplained variance, relative to unconstrained regression. Non-negative matrix factorization is not an exact factorization, but rather an approximation with a residual error component. Forcing non-negativity on the decomposition of predictor and response variables is necessary for analysis, but produces less than ideal results by introducing this error.

Other improvements are needed in the analysis of spectroscopic data. Our analysis thus far has relied on the tentative assignment of Raman bands to biochemicals based on work from independent studies. While this practice is not an unusual tactic, it is highly presumptive and only aids in drawing hypothesis regarding spectral occurrences, rather than solid conclusions. To better affirm these assignments, it is necessary to isolate and observe the chemical components of relevant pathobiological events. For example, one might assess the action of cABC on a solution of isolated CS or CSPG molecules. *In situ* spectral occurrences could then be compared to those of the cABC-CS/CSPG solution, so as to elucidate which occurrences were a direct result of the enzyme-substrate interaction and which were auxiliary. Additionally, a similar comparison could be performed using the spectra of activated glial cells in isolation of an extracellular matrix. This would help elucidate which spectral occurrences correlate specifically to cells versus the extracellular matrix, further identifying their source.

One major disadvantage of the organotypic model is its lack of long-term viability. Reports show organotypic cultures of spinal cord tissue only maintain viability for an average of 2 weeks.<sup>20,22,50,51</sup> Thus, to assess treatment over the full timeframe of SCI, the next major step for this work is *in vivo* experimentation. Ideally, injury and treatment

will be performed in a surgical setting, and the animal will be allowed a subsequent period of recovery. Herein lie two divergent paths that may be taken. Spectroscopic analysis will be performed either on excised sections of tissue, which requires euthanasia, or on the living animal as a whole. The latter is ideal, in that it mimics clinical applications, but it presents a wide-range of challenges, including imaging through bone and connective tissue, imaging in a vascularized environment, and anesthetizing the animal during imaging, to name a few. However, despite these challenges it is intriguing to consider RS for the clinical assessment of cABC SCI treatment. Furthermore, the generation of an *in vivo* model using a mouse would allow a more precise assessment the organotypic model's ability to recapitulate major pathobiological events of SCI. While data in this study largely agreed with data of our previous *in vivo* model<sup>16</sup>, said model was constructed using an entirely different model organism, the rat. Cross-species comparison is useful in providing insight to the similarities between the models; however there is little way of inferring which differences correlate to the species and which to the models.

## REFERENCES

1. Bradbury, E.J., Moon, L.D.F., Popat, R.J., King, V.R., Bennett, G.S., Patel, P.N., Fawcett, J.W., McMahon, S.B. Chondroitinase ABC promotes functional recovery after spinal cord injury (2002) *Nature*, 416 (6881), pp. 636-640.
2. McKeon, R. J., Schreiber, R. C., Rudge, J. S. & Silver, J. Reduction of neurite outgrowth in a model of glial scarring following CNS injury is correlated with the expression of inhibitory molecules on reactive astrocytes. (1991) *J. Neurosci.* 11, pp. 3398–3411.
3. Smith-Thomas, L. C. et al. An inhibitor of neurite outgrowth produced by astrocytes. (1994) *J. Cell Sci.* 107, pp. 1687–1695.
4. National Spinal Cord Injury Statistical Center, Spinal cord injury facts and figures at a glance (Birmingham, Alabama, 2012), [https://www.nscisc.uab.edu/PublicDocuments/fact\\_figures\\_docs/Facts%202012%20Feb%20Final.pdf](https://www.nscisc.uab.edu/PublicDocuments/fact_figures_docs/Facts%202012%20Feb%20Final.pdf)
5. Pekny, M., Nilsson, M. Astrocyte activation and reactive gliosis (2005) *GLIA*, 50 (4), pp. 427-434.
6. Kimura-Kuroda, J., Teng, X., Komuta, Y., Yoshioka, N., Sango, K., Kawamura, K., Raisman, G., Kawano, H. An in vitro model of the inhibition of axon growth in the lesion scar formed after central nervous system injury (2010) *Molecular and Cellular Neuroscience*, 43 (2), pp. 177-187.
7. East, E., Golding, J.P., Phillips, J.B. A versatile 3D culture model facilitates monitoring of astrocytes undergoing reactive gliosis (2009) *Journal of Tissue Engineering and Regenerative Medicine*, 3 (8), pp. 634-646.
8. Siebert, J.R., Stelzner, D.J., Osterhout, D.J. Chondroitinase treatment following spinal contusion injury increases migration of oligodendrocyte progenitor cells (2011) *Experimental Neurology*, 231 (1), pp. 19-29.
9. Horner, P.J., Gage, F.H. Regenerating the damaged central nervous system (2000) *Nature*, 407 (6807), pp. 963-970.
10. Sharma, K., Selzer, M.E., Li, S. Scar-mediated inhibition and CSPG receptors in the CNS (2012) *Experimental Neurology*, 237 (2), pp. 370-378.
11. Moon, L.D.F., Asher, R.A., Rhodes, K.E., Fawcett, J.W. Regeneration of CNS axons back to their target following treatment of adult rat brain with chondroitinase ABC (2001) *Nature Neuroscience*, 4 (5), pp. 465-466.
12. Mountney, A., Zahner, M.R., Sturgill, E.R., Riley, C.J., Aston, J.W., Oudega, M., Schramm, L.P., Hurtado, A., Schnaar, R.L. Sialidase, chondroitinase ABC, and combination therapy after spinal cord contusion injury (2013) *Journal of Neurotrauma*, 30 (3), pp. 181-190.

13. Tuinstra, H.M., Ducommun, M.M., Briley, W.E., Shea, L.D. Gene delivery to overcome astrocyte inhibition of axonal growth: An in vitro Model of the glial scar (2013) *Biotechnology and Bioengineering*, 110 (3), pp. 947-957.
14. García-Alías, G., Fawcett, J.W. Training and anti-CSPG combination therapy for spinal cord injury (2012) *Experimental Neurology*, 235 (1), pp. 26-32.
15. Krafft, C., Sergo, V. Biomedical applications of Raman and infrared spectroscopy to diagnose tissues (2006) *Spectroscopy*, 20 (5-6), pp. 195-218.
16. Saxena, T., Deng, B., Stelzner, D., Hasenwinkel, J., Chaiken, J. Raman spectroscopic investigation of spinal cord injury in a rat model (2011) *Journal of Biomedical Optics*, 16 (2), art. no. 027003.
17. Galli, R., Uckermann, O., Winterhalder, M.J., Sitoci-Ficici, K.H., Geiger, K.D., Koch, E., Schackert, G., Zumbusch, A., Steiner, G., Kirsch, M. Vibrational spectroscopic imaging and multiphoton microscopy of spinal cord injury (2012) *Analytical Chemistry*, 84 (20), pp. 8707-8714.
18. Morrison, B., Elkin, B.S., Dollé, J.-P., Yarmush, M.L. In vitro models of traumatic brain injury (2011) *Annual Review of Biomedical Engineering*, 13, pp. 91-126.
19. Zhang, J., O'Carroll, S.J., Wu, A., Nicholson, L.F.B., Green, C.R. A model for ex vivo spinal cord segment culture-A tool for analysis of injury repair strategies (2010) *Journal of Neuroscience Methods*, 192 (1), pp. 49-57.
20. Cifra, A., Mazzone, G.L., Nani, F., Nistri, A., Mladinic, M. Postnatal developmental profile of neurons and glia in motor nuclei of the brainstem and spinal cord, and its comparison with organotypic slice cultures (2012) *Developmental Neurobiology*, 72 (8), pp. 1140-1160.
21. Zhang, H., Bennett, J.L., Verkman, A.S. Ex vivo spinal cord slice model of neuromyelitis optica reveals novel immunopathogenic mechanisms (2011) *Annals of Neurology*, 70 (6), pp. 943-954.
22. Avossa, D., Rosato-Siri, M.D., Mazzarol, F., Ballerini, L. Spinal circuits formation: A study of developmentally regulated markers in organotypic cultures of embryonic mouse spinal cord (2003) *Neuroscience*, 122 (2), pp. 391-405.
23. Stoppini, L., Buchs, P.-A., Muller, D. A simple method for organotypic cultures of nervous tissue (1991) *Journal of Neuroscience Methods*, 37 (2), pp. 173-182.
24. Krassioukov, A.V., Ackery, A., Schwartz, G., Adamchik, Y., Liu, Y., Fehlings, M.G. An in vitro model of neurotrauma in organotypic spinal cord cultures from adult mice (2002) *Brain Research Protocols*, 10 (2), pp. 60-68.
25. Saxena, T., Deng, B., Lewis-Clark, E., Hoellger, K., Stelzner, D., Hasenwinkel, J., Chaiken, J. Near infrared Raman spectroscopic study of reactive gliosis and the glial scar in injured rat spinal cords (2010) *Progress in Biomedical Optics and Imaging - Proceedings of SPIE*, 7560, art. no. 75600I.

26. Sowa, M.G., Smith, M.S.D., Kendall, C., Bock, E.R., Alex, C.-T.K.O., Choo-Smith, L.-P., Stone, N. Semi-parametric estimation in the compositional modeling of multicomponent systems from Raman spectroscopic data (2006) *Applied Spectroscopy*, 60 (8), pp. 877-883.
27. Labombarda, F., Ghoumari, A.M., Liere, P., De Nicola, A.F., Schumacher, M., Guennoun, R. Neuroprotection by steroids after neurotrauma in organotypic spinal cord cultures: A key role for progesterone receptors and steroidal modulators of GABAA receptors (2013) *Neuropharmacology*, 71, pp. 46-55.
28. Krafft, C., Neudert, L., Simat, T., Salzer, R. Near infrared Raman spectra of human brain lipids (2005) *Spectrochimica Acta - Part A: Molecular and Biomolecular Spectroscopy*, 61 (7), pp. 1529-1535.
29. Tsuboi, M., Ezaki, Y., Aida, M., Suzuki, M., Yimit, A., Ushizawa, K., Ueda, T. Raman scattering tensors of tyrosine (1998) *Biospectroscopy*, 4 (1), pp. 61-71.
30. Chan, J.W., Taylor, D.S., Zwerdling, T., Lane, S.M., Ihara, K., Huser, T. Micro-Raman spectroscopy detects individual neoplastic and normal hematopoietic cells (2006) *Biophysical Journal*, 90 (2), pp. 648-656.
31. Stone, N., Hart Prieto, M.C., Crow, P., Uff, J., Ritchie, A.W. The use of Raman spectroscopy to provide an estimation of the gross biochemistry associated with urological pathologies (2007) *Analytical and Bioanalytical Chemistry*, 387 (5), pp. 1657-1668.
32. Movasaghi, Z., Rehman, S., Rehman, I.U. Raman spectroscopy of biological tissues (2007) *Applied Spectroscopy Reviews*, 42 (5), pp. 493-541.
33. Bansil, R., Yannas, I.V., Stanley, H.E. Raman spectroscopy: A structural probe of glycosaminoglycans (1978) *Biochimica et Biophysica Acta*, 541 (4), pp. 535-542.
34. Arboleda, P.H., Loppnow, G.R. Raman spectroscopy as a discovery tool in carbohydrate chemistry (2000) *Analytical Chemistry*, 72 (9), pp. 2093-2098.
35. Bell, A.F., Barron, L.D., Hecht, L. Vibrational Raman optical activity study of D-glucose (1994) *Carbohydrate Research*, 257 (1), pp. 11-24.
36. Ellis, R., Green, E., Winlove, C.P. Structural analysis of glycosaminoglycans and proteoglycans by means of Raman microspectrometry (2009) *Connective Tissue Research*, 50 (1), pp. 29-36.
37. Horiba, Raman data and analysis: Raman spectroscopy for analysis and monitoring (Edison, New Jersey 2013),  
<http://www.horiba.com/fileadmin/uploads/Scientific/Documents/Raman/bands.pdf>
38. Iaci, J.F., Vecchione, A.M., Zimber, M.P., Caggiano, A.O. Chondroitin sulfate proteoglycans in spinal cord contusion injury and the effects of chondroitinase treatment (2007) *Journal of Neurotrauma*, 24 (11), pp. 1743-1759.

39. Jones, L.L., Margolis, R.U., Tuszynski, M.H. The chondroitin sulfate proteoglycans neurocan, brevican, phosphacan, and versican are differentially regulated following spinal cord injury (2003) *Experimental Neurology*, 182 (2), pp. 399-411.
40. Zhang, Z., Park, Y., Kemp, M.M., Zhao, W., Im, A.-R., Shaya, D., Cygler, M., Kim, Y.S., Linhardt, R.J. Liquid chromatography-mass spectrometry to study chondroitin lyase action pattern (2009) *Analytical Biochemistry*, 385 (1), pp. 57-64.
41. Moore, K.L. Protein tyrosine sulfation: A critical posttranslation modification in plants and animals (2009) *Proceedings of the National Academy of Sciences of the United States of America*, 106 (35), pp. 14741-14742.
42. Spitzbarth, I., Bock, P., Haist, V., Stein, V.M., Tipold, A., Wewetzer, K., Baumgärtner, W., Beineke, A. Prominent microglial activation in the early proinflammatory immune response in naturally occurring canine spinal cord injury (2011) *Journal of Neuropathology and Experimental Neurology*, 70 (8), pp. 703-714.
43. Wu, D., Ingram, A., Lahti, J.H., Mazza, B., Grenet, J., Kapoor, A., Liu, L., Kidd, V.J., Tang, D. Apoptotic release of histones from nucleosomes (2002) *Journal of Biological Chemistry*, 277 (14), pp. 12001-12008.
44. Kutcher, M.E., Xu, J., Vilardi, R.F., Ho, C., Esmon, C.T., Cohen, M.J. Extracellular histone release in response to traumatic injury: Implications for a compensatory role of activated protein C (2012) *Journal of Trauma and Acute Care Surgery*, 73 (6), pp. 1389-1394.
45. Bergholt, M.S., Wei, Z., Lin, K., Ho, K.Y., Ming, T., Yeoh, K.G., So, J.B.Y., Huang, Z. Characterizing variability in in vivo Raman spectra of different anatomical locations in the upper gastrointestinal tract toward cancer detection (2011) *Journal of Biomedical Optics*, 16 (3), art. no. 037003.
46. Stone, N., Hart Prieto, M.C., Crow, P., Uff, J., Ritchie, A.W. The use of Raman spectroscopy to provide an estimation of the gross biochemistry associated with urological pathologies (2007) *Analytical and Bioanalytical Chemistry*, 387 (5), pp. 1657-1668.
47. Painter, P.C., Koenig, J.L. Interpretation of hypochromic and hyperchromic intensity changes in the Raman spectra of polypeptides and polynucleotides undergoing transition (1976) *Biopolymers*, 15 (2), pp. 241-255.
48. Aubrey, K.L., Casjens, S.R., Thomas Jr., G.J. Secondary structure and interactions of the packaged dsDNA genome of bacteriophage P22 investigated by Raman difference spectroscopy (1992) *Biochemistry*, 31 (47), pp. 11835-11842.

49. Chiba, K., Masuda, K., Andersson, G.B.J., Momohara, S., Thonar, E.J. Matrix replenishment by intervertebral disc cells after chemonucleolysis in vitro with chondroitinase ABC and chymopapain (2007) *Spine Journal*, 7 (6), pp. 694-700.
50. Cho, J.-S., Park, H.-W., Park, S.-K., Roh, S., Kang, S.-K., Paik, K.-S., Chang, M.-S. Transplantation of mesenchymal stem cells enhances axonal outgrowth and cell survival in an organotypic spinal cord slice culture (2009) *Neuroscience Letters*, 454 (1), pp. 43-48.
51. Guzmán-Lenis, M.-S., Vallejo, C., Navarro, X., Casas, C. Analysis of FK506-mediated protection in an organotypic model of spinal cord damage: Heat shock protein 70 levels are modulated in microglial cells (2008) *Neuroscience*, 155 (1), pp. 104-113.

## **VITA**

NAME OF AUTHOR: Shane Ruberto

PLACE OF BIRTH: Pittsfield, Massachusetts

DATE OF BIRTH: December 7<sup>th</sup>, 1988

UNDERGRADUATE SCHOOL ATTENDED: Syracuse University

DEGREE AWARDED: Bachelor of Science in Biomedical Engineering, May 2011

### **AWARDS AND HONORS:**

Dean's List, Syracuse University, 2007-2011

University Honors (Magna Cum Laude), Syracuse University, 2011

### **PROFESSIONAL EXPERIENCE:**

Research Assistant, Department of Biomedical and Chemical Engineering, Syracuse University, 2011-2013